Received: 28 May 2021 | Revised: 12 February 2022 | Accepted: 21 March 2022

DOI: 10.1111/mec.16457

ORIGINAL ARTICLE

MOLECULAR ECOLOGY WILEY

Fine-scale genome-wide signature of Pleistocene glaciation in *Thitarodes* moths (Lepidoptera: Hepialidae), host of *Ophiocordyceps* fungus in the Hengduan Mountains

Zhengyang Wang | Naomi E. Pierce

Museum of Comparative Zoology and Department of Organismic and Evolutionary Biology, Harvard University, Cambridge, Massachusetts, USA

Correspondence
Zhengyang Wang and Naomi E. Pierce, Museum of Comparative Zoology and Department of Organismic and Evolutionary Biology, Harvard University, Cambridge, MA 02138, USA.
Emails: zhengyangw@hotmail.com (Z.W.); npierce@oeb.harvard.edu (N.E.P.)

Funding information
NSF, Grant/Award Number: NSF DEB 1541560

Handling Editor: Tara Pelletier

Abstract

The Hengduan Mountains region is a biodiversity hotspot known for its topologically complex, deep valleys and high mountains. While landscape and glacial refugia have been evoked to explain patterns of interspecies divergence, the accumulation of intra-species (i.e., population level) genetic divergence across the mountain-valley landscape in this region has received less attention. We used genome-wide restriction site-associated DNA sequencing (RADseq) to reveal signatures of Pleistocene glaciation in populations of *Thitarodes shambalaensis* (Lepidoptera: Hepialidae), the host moth of parasitic *Ophiocordyceps sinensis* (Hypocreales: Ophiocordycipitaceae) or "caterpillar fungus" endemic to the glacier of eastern Mt. Gongga. We used moraine history along the glacier valleys to model the distribution and environmental barriers to gene flow across populations of *T. shambalaensis*. We found that moth populations separated by less than 10 km exhibited valley-based population genetic clustering and isolation-by-distance (IBD), while gene flow among populations was best explained by models using information about their distributions at the local last glacial maximum (LGM_L, 58 kya), not their contemporary distribution. Maximum likelihood lineage history among populations, and among subpopulations as little as 500 m apart, recapitulated glaciation history across the landscape. We also found signals of isolated population expansion following the retreat of LGM_L glaciers. These results reveal the fine-scale, long-term historical influence of landscape and glaciation on the genetic structuring of populations of an endangered and economically important insect species. Similar mechanisms, given enough time and continued isolation, could explain the contribution of glacier refugia to the generation of species diversity among the Hengduan Mountains.

KEYWORDS
caterpillar fungus, glaciation, Hengduan Mountains, landscape genomics, last glacial maximum, population genetics

1 | INTRODUCTION

Climatic oscillations from the late Pleistocene (130–11 kya) glaciation and subsequent Holocene warming left their signatures on the genetic structuring of many species around the world (Bagley et al., 2017; Devitt et al., 2013; Dudaniec et al., 2012; Marske et al., 2020; Wachter et al., 2016; Yannic et al., 2014). The signature of population responses to glacial expansion and subsequent retreat since the last glacial maximum (LGM, 26 kya) are especially well-documented. During periods of extensive glaciation, large ice sheets sometimes acted as direct barriers of gene flow that caused population divergence (Marske et al., 2020). While some species persisted in periglacial refugia (Escobar García et al., 2012), others remained at high-elevation ice-free "nunataks", resulting in deep divergence between populations (Stehlik et al., 2002). Post LGM, some populations colonized newly available ice-free habitats and showed a signal of immediate population expansion (Wachter et al., 2016); or some populations declined due to founder effects (Wang et al., 2020). These demographic responses are not mutually exclusive; the genetic signatures of glaciation are often taxa and region-specific. To date, the majority of studies on genetic signatures of Pleistocene glaciation have been conducted in North America and Northern Europe (for review see Wallis et al., 2016). By contrast, the eastern Himalayas and Hengduan Mountains house an estimated 40,800 km^2 of existing glaciers (which account for up to 70% of the seasonal water flow of the region, Xu et al., 2009; Bolch et al., 2012), but the genetic signatures of historical glaciation on divergent populations of this region have rarely been investigated.

The Hengduan Mountains region (also known as the "eastern Himalayas" or the "mountains of southwest China") is a global biodiversity hotspot (Marchese, 2015). The region is known for topologically complex deep valleys and high mountains. In explaining the extraordinary *Rhododendron* diversity of the region (more than 50% of the world's existing species), Irving and Hebda (1993) postulated that species inhabiting a deep valley diverged in response to recurrent glacial-interglacial climate changes. While insect diversity in the region is largely understudied (Ji et al., 2013; Liu et al., 2020), recent studies on the distribution of plants and vertebrates confirmed the presence of a Pleistocene glacial barrier and refugia across the entire range of Hengduan-Himalaya (Meng et al., 2015; Qiu et al., 2011; Wan et al., 2021). Most studies of biodiversity in the region have addressed the process of interspecies divergence, while the "missing link" lies in explaining the accumulation of intraspecific genetic diversity across the mountain-valley landscape.

We here focus on the process of population divergence of the ghost moth, *Thitarodes shambalaensis* (Lepidoptera: Hepialidae, Wang et al., 2019), which is endemic to pockets of high elevation alpine meadows inside the seven valleys of Mt. Gongga (29°35′45″N, 101°52′45″E), the highest peak (7556 m) in the Hengduan Mountains (Figure 1). In the following introduction we first review how genetic divergence is spatially and temporally-explicitly modelled in complex landscapes, then we introduce how these methods are relevant to our specific study system of *T. shambalaensis* at Mt. Gongga using historical moraine records.

1.1 | Measuring population divergence across complex landscapes

Landscape genetics examine how geographical and environmental features shape population structure along spatial and temporal axes (Manel et al., 2003). On the spatial axis, geographical and environmental variation may limit an individual's ability to disperse (Kidd & Ritchie, 2006). The resulting genetic divergence among distant populations due to reduced gene flow and random drift is called "isolation by dispersal limitation" (IBDL). Populations under IBDL exhibit patterns of isolation-by-distance (IBD), whereby genetic differences between populations are positively correlated with their geographic Euclidean distances (Wright, 1931) or log-transformed equivalent in 2D models (Rousset, 1997). Since IBD is not the result of natural selection, it can be readily measured with genetically neutral markers such as microsatellites (Vieira et al., 2016) and restriction site-associated DNA sequencing (RADseq, Andrews et al., 2016) generating single nucleotide polymorphisms (SNPs) that are parsed from adaptive outliers. Distance-isolated populations are often confirmed by statistical correlations among population genetic distances and geographical distances, and further analysed through ancestry-based genetic clustering and coalescent-based genetic modelling. IBD has been confirmed in studies of species with expansive distributions (recent examples include Bagley et al., 2017; Lanier et al., 2015; Rutherford et al., 2021; Van Buskirk & Jansen van Rensburg, 2020), and is often taken as a "null hypothesis" in the genetic structuring of widespread populations (Orsini et al., 2013).

However, IDB alone does not capture the heterogeneity of the landscape that individuals must traverse. For instance, the experience of dispersal for land-dwellers moving across mountain valleys is different from that of marine organisms swimming through the ocean. While empirical "least cost paths" are sometimes used to substitute Euclidean distance to obtain a more practical model of gene flow (Arnaud, 2003), isolation-by-resistance (IBR, McRae, 2006), a modification of IBD that uses environmental variables to parameterize the "resistance" individuals experience in dispersal across the landscape, can typically achieve a more accurate model of genetic differentiation (McRae & Beier, 2007; Shirk et al., 2010, van Etten & Hijmans, 2010, but see MacDonald et al., 2020). IBR applies circuit theory to solve for the most probable path of dispersal (that is, the path with least resistance, McRae et al., 2008).

IBD models also fail to account for local adaptation. In cases of isolation-by-adaptation (IBA; Nosil & Crespi, 2004; Nosil et al., 2009), adaptation to local environments leads to a reduced tendency for individuals to disperse across a variable environmental gradient. This results in genetic patterns of isolation-by-environment (IBE; Wang & Summers, 2010), where controlling for IBD/IBR-induced genetic variation, populations occupying the same environment are

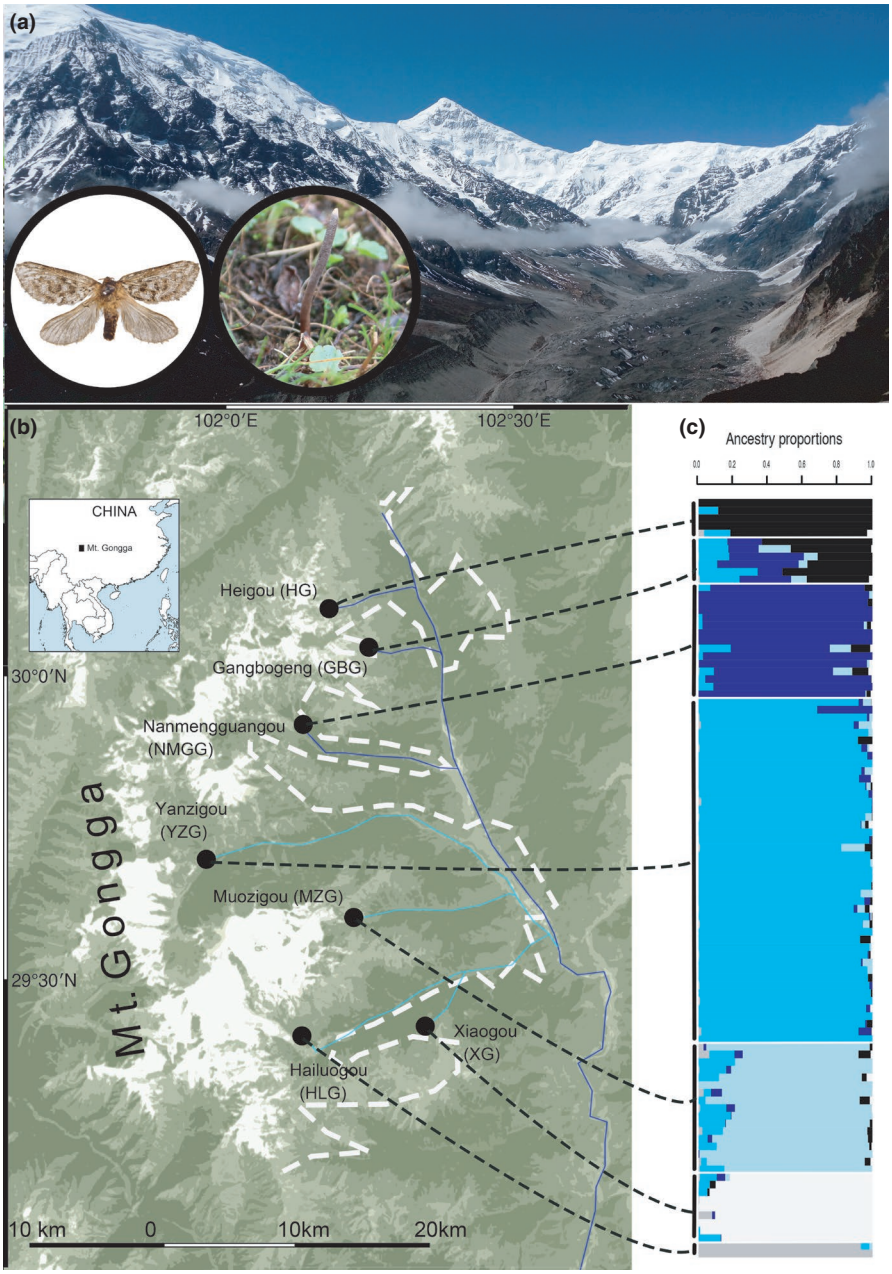

FIGURE 1 Populations of *T. shambalaensis* sampled in this study. (a) *T. shambalaensis* habitat in Yanzigou glacier valley leading from peak of Mt. Gongga, China. Circled inserts show a *T. shambalaensis* adult and a "caterpillar fungus" *O. sinensis*. (b) Sample localities in seven glacier valleys along the eastern slope of Mt. Gongga. Contemporary glaciers and snow cover are indicated in white. The extent of historical glaciers at the local last glacial maximum is delineated by white dotted lines. Northern valleys drain individually into the Moxi river along the Kangding-Moxi fault line (dark blue); southern valleys shared a historical ice sheet and common drainage (light blue) before merging with Moxi river. (c) Results of sNMF analysis for best fit $K = 6$. Each row is an individual ($n = 99$); six different colours represent admixture of genetic clusters

more similar to each other than those in different environments. Empirically, populations that are separated by geographical distances (IBD/IBR) often inhabit different environments (IBE), making it difficult to determine which process drove the diversification within a given species. Qualitative methods have been developed to assess the relative contribution of environment and geography to genetic structure (Bradburd et al., 2013; Wang et al., 2013). A number of studies have found that a combination of IBD/IBR and IBE best explains existing genetic variation among populations (Bagley et al., 2017; Dudaniec et al., 2012; Fant et al., 2014; Rutherford et al., 2021; Smith et al., 2019; Van Buskirk & Jansen van Rensburg, 2020).

The second, temporal axis of landscape genetics, emphasizes that extant population differentiation is the historical average of gene flow over a long period of time (Bradburd & Ralph, 2019). Prominent topological features of the landscape such as drainage systems and mountains set hard boundaries of population gene flow (Mayr, 1942), while historical fluctuations in climate alter the habitable range, and thus the resistance landscape, of gene flow (Vasconcellos et al., 2019). Populations often exhibit patterns of isolation-by-history (IBH), in which contemporary patterns of genetic structure (or measurable gene flow between populations) reflect historical habitat ranges or orogenesis boundaries that are no longer present (Marske et al., 2020; Moreira et al., 2020; Silva et al., 2021; Vasconcellos et al., 2019).

The dual spatial and temporal considerations in landscape genetics call for models of gene flow that are explicit in the distribution of populations, their pedigrees, and their environmental landscapes past and present (Bradburd & Ralph, 2019). Some recent studies specify historical population distributions and dispersal landscapes in agent-based, spatially-explicit simulations (Becheler et al., 2019;

Currat et al., 2019) and leverage approximate Bayesian methods (Wegmann et al., 2010) to select for historical scenarios that best explain empirical genetic structure (Bemmels et al., 2016; Brown & Knowles, 2012; He et al., 2013; Lacey Knowles & Alvarado-Serrano, 2010; Massatti & Knowles, 2016). Studies also use coalescent-based methods (Excoffier et al., 2013) that start with current genetic compositions and simulate pedigree backwards in time, with prior parameters that reflect gene flow restrictions due to historical events (Bagley et al., 2017; Lanier et al., 2015; Moreira et al., 2020; Myers et al., 2020). Both the spatially-explicit simulation approach and the coalescent approach often combine genomic data with environmental niche modelling (ENM) to infer potential population distributions and barriers to gene flow (Carstens & Richards, 2007), and are generally referred to as integrated distributional, demographic and coalescent (iDDC; He et al., 2013) modelling approaches.

These spatially and temporally explicit genomic simulations are usually conducted on populations with wide-ranging, well-documented distributions in environmentally variable habitats. At more refined spatial scales (e.g., populations within 10 km of each other), the resolution of paleoclimate data is not sufficient for ENM. Paleoclimate data for ENM are limited to 2.5 arc min (4.6 km at 0 latitude) for most time periods (Fordham et al., 2017), and at best 30 arc sec (0.93 km at 0 latitude) for the last glacial maximum (Karger et al., 2017). If genetic structure exists at a finer scale than ENM allows, researchers often rely on known changes in immediate environment or historical events to formulate their coalescent hypotheses (Geng et al., 2009; Helsen et al., 2015; Hevroy et al., 2018; Kitamura et al., 2018; Kobayashi et al., 2018; Pearson et al., 2020; Ziege et al., 2020).

1.2 | Study system

We focus on the process of population divergence across seven glacial valleys of Mt. Gongga (Figure 1). The valleys drain into the Moxi river, which runs along a fault line (Kangding-Moxi fault) east of Mt. Gongga. The valleys extend 30 km from north to south, with parallel neighbouring valleys less than 10 km from each other. ENM at this scale is difficult, but the extent of ice sheet retreat from the last local glacial maximum to the present day has been inferred by moraine dating (Li et al., 2010; Pan et al., 2012; Wang, Pan, et al., 2013). The local glaciation history relevant to this study includes: (1) the local last glacial maximum (LGM_L) at Mt. Gongga occurred about 58 kya, considerably earlier than the 26 kya timing of the “global” LGM in Europe and North America (Clark et al., 2009). At LGM_L, an ice sheet extended from the peak of Mt. Gongga to the Kangdi-Moxi fault. (2) The path of retreat of the post-LGM_L ice sheet overlaps with creation of present day river valleys, suggesting that these valleys were gradually carved out during the retreat process. (3) Rivers in the northern valleys of Heigou (HG), Gangbogeng (GBG), Nanmengguangou (NMGG) drain directly into the Moxi river (Figure 1b, dark blue lines), while the southern valleys of Yanzigou (YZG), Muozigou (MZG), Hailuogou (HLG) and Xiaogou (XG) belonged to the same expansive ice sheet during LGM_L. Rivers in the southern valleys merge into a single river before joining the Moxi river (Figure 1b, light blue lines). These regional histories allow us to test specific hypotheses of population divergence in the region.

Populations of the ghost moth, *Thitarodes shambalaensis*, (Lepidoptera: Hepialidae, Wang, Zhuang, et al., 2019) are endemic to pockets of high elevation alpine meadows inside the seven valleys of Mt. Gongga (Table S1). The full life history of *T. shambalaensis* has never been documented, but is likely to be similar to other species of *Thitarodes* that live in high elevation meadows (3600–5000 m) of the Himalaya and Hengduan Mountains (Chu et al., 2004; Wang & Yao, 2011). These moths have strict habitat requirements (Hopping et al., 2018; Wang et al., 2020) and low vagility due to their short period of adult activity (Maczey et al., 2010; Zou et al., 2011): larvae develop under the soil and can take 1–1.5 years to become adults (Tao et al., 2016), which emerge, mate and lay eggs over a brief 1–2 week period in the summer months. *Thitarodes* larvae are sometimes parasitized by the fungus, *Ophiocordyceps sinensis*, (order Hypocreales; family Ophiocordycipitaceae), resulting in a fungal mycelium-insect exoskeleton complex commonly called "caterpillar fungus" (Sung et al., 2007; Shrestha et al., 2014). Caterpillar fungi have been collected across the Himalaya-Hengduan region as ethnobotanical medicine since the 15th century (Winkler, 2008, 2010). Recent molecular evidence suggests that *Thitarodes* across the Himalaya-Hengduan region diverged into roughly 50 species along major landscape barriers and coevolved with their parasitic fungal strains (Quan et al., 2014; Zhang et al., 2014). However, fine-scale population-level divergence within a single species of *Thitarodes* has yet to be investigated. The distribution of *T. shambalaensis* populations in glacial valleys of Mt. Gongga is interesting because contemporary populations, each located in a small "pocket" or cul de sac at the end of a glacier (i.e., at the head of a river valley), are separated by less than 10 km of Euclidean distance (Figure 1b), but the mountains flanking each valley and dividing each population are likely to be major dispersal barriers (Wang et al., 2019) that confine isolated populations within a relatively small valley habitat. We hypothesized that *T. shambalaensis* populations arrived at their current isolated habitats from a more connected landscape following the retreating ice sheet post-LGM_L, and that their contemporary genetic structure should reflect a combination of landscape topology (IBR) and historical glaciation events (IBH).

We used genome-wide SNPs to investigate population structure of *T. shambalaensis*. (1) First, we explored the genetic clustering among individuals of *T. shambalaensis*. We hypothesized that because valleys are topological dispersal barriers, valley-based genetic structure should exist among individuals, even when distances across valleys are less than 10 km. Further focusing onto a single valley, we asked whether glacier-influenced genetic structure is also detectable between subpopulations on two sides of the same glacial valley, only 500 m apart. If such a fine-grained signal exists, the effect of IBD alone would lead us to expect population genetic clustering among nearby samples on the same side of the valley, while a historical view of population invasion would predict genetic clustering according to sample proximity to the glacier tongue, regardless

of the side of the valley they inhabit. (2) Second, we reconstructed lineage histories among populations. We hypothesized that contemporary lineages in valleys carved out by the same historical ice sheet form a single monophyletic cluster. (3) Third, we modelled historical population distributions using fine-scale moraine dating, and used this to infer the earlier migration landscape, differentially prioritizing the effect of isolation (IBD), topology (IBR) and environment (IBE). To do this, we incorporated moraine-based historical distance sets as migration parameters in coalescent simulations. We then evaluated whether these refinements provide better estimates of contemporary genetic structure. To further explore the demographic dynamics derived from moraine-based models, we also modelled the divergence time and migration time of each population separately. We tested the hypothesis that populations of *T. shambalaensis* underwent historical migration around LGM_L, followed by population expansion in relative isolation during the subsequent glacial retreat.

2 | MATERIALS AND METHODS

2.1 | Sampling, sequencing and SNP calling

Between May and June of 2016 and 2017, we collected 122 *T. shambalaensis* from caterpillar fungus habitats (3822–4080 m) in the seven valleys of eastern Mt. Gongga (Figure 1b, Tables S1 and S2, see Wang et al., 2020 for habitat description). We excavated *T. shambalaensis* pupae and larvae from multiple 50 × 50 × 30 cm sampling plots that were each 100 m apart (uprooted vegetation was placed back after sampling). We also netted adults at dusk. We obtained from 2 to 45 samples per valley (Table S1, mean = 16.7, SD = 13.8). At least 100 ng of genomic DNA was extracted from each sample using Qiagen DNeasy Blood and Tissue Kits (Qiagen Inc.). Samples were sent for RADseq at 1GENE Inc., Hangzhou, China. We followed the RADseq protocol of Etter et al. (2011). Briefly, DNA was digested with *Eco*RI restriction enzymes, ligated with Illumina adaptor sequences and unique 5-base pair barcodes, and size-selected for 300–500 base pairs. Ligated fragments were PCR-amplified and sequenced on Illumina HiSeq4000 to generate paired-end 150 base pair reads (demultiplexed raw data available on Dryad: https://doi.org/10.5061/dryad.v41ns1rzm).

Demultiplexed sequences were cleaned by removing reads that had Phred quality scores lower than 10 for over 50% of their base pairs. Reads were assembled *de novo* following the STACKS pipeline (Rochette & Catchen, 2017). We started by grouping reads with a minimum coverage depth from a single individual into unique stacks. We then removed stacks that were repetitive (using the program USTACKS). We called SNPs on each locus following a multinomial-based likelihood model (Catchen et al., 2013), and compiled a catalogue of consensus loci among all individuals (program CSTACKS). We targeted a minimum coverage of three reads for a stack and allowed a two base pair mismatch between each stack (a conservative approach to delineating loci, see Rochette and Catchen (2017). Stacks with no more than one base pair mismatch across individuals were merged into consensus loci. Alleles from each individual were then called against the consensus loci catalogue in the program SSTACKS. To identify missing data, we used an approach similar to that of de Medeiros and Farrell (2018) to visualize the presence/ absence of each SNP for all individuals after hierarchical clustering (Ward, 1963). The resulting matrix (Figure S1) identified individuals with highly degraded DNA as well as those with enzymatic cut sites not shared by most *T. shambalaensis*. We also cross-referenced these data with an independently derived CO1-based phylogeny to remove any misidentified individuals that were not monophyletic with *T. shambalaensis* (see Wang, Zhuang, et al., 2019 for details). After removing these individuals, we used the "-r" option of the POPULATIONS program in STACKS to select loci with less than 10% missing data across all individuals. We included 1 SNP per locus to minimize linkage disequilibrium (LD) between SNPs.

2.2 | Population structure and phylogeny

We calculated the nucleotide diversity (θ, estimated as π), observed and expected heterozygosity (H_{obs} and H_{exp}) and inbreeding coefficient (F_{IS}) for each population using the POPULATIONS program in STACKS to examine possible correlations between environmental variables and population genetic diversity (Table 1), whereas these population diversity-related variables might correlate with historical habitat stability (Yannic et al., 2014; Ortego et al., 2015). For each SNP, we applied a Hardy-Weinberg Equilibrium (HWE) test for multilocus data to look for deviation from HWE within each population (function HWE.test implemented in R package adegenet, Jombart, 2008). We checked whether the latitude, longitude, elevation and sample size of each population correlated with its diversity and F_{IS}.

TABLE 1 Population summary statistics from 2373 RADseq loci, calculated separately for each population, including number of sample genotyped per population (*N*), average observed and expected heterozygosity per locus (H_{obs} and H_{exp}), average nucleotide diversity per locus (π), Wright's inbreeding coefficient (F_{IS}) and mean frequency of the most frequent allele per locus (*p*)

	N	H_{obs}	H_{exp}	π	F_{IS}	$p \pm SD$
Heigou (HG)	5	0.2465	0.3046	0.3384	0.2136	0.7858 ± 0.0011
Gangbogeng (GBG)	6	0.2046	0.2726	0.2974	0.2327	0.8145 ± 0.0007
Nanmengguangou (NMGG)	15	0.1492	0.1810	0.1875	0.1441	0.8823 ± 0.0009
Yanzigou (YZG)	45	0.0670	0.0672	0.0680	0.0680	0.9587 ± 0.0013
Muozigou (MZG)	17	0.1031	0.1356	0.1400	0.1712	0.9173 ± 0.0009
Xiaogou (XG)	9	0.1492	0.1974	0.2090	0.1978	0.8747 ± 0.0007
Hailuogou (HLG)	2	0.4536	0.4176	0.5568	0.1549	0.6648 ± 0.0004

Nei's pairwise F_{ST} between all populations was calculated with the pairwise.fst function in R package adegenet (Jombart, 2008). To test for IBD, we applied Mantel tests (Mantel, 1967) to look for any correlation between population pairwise F_{ST} and geographic Euclidean distance. While fine-scale climatic variables are not available at the resolution of individual habitats, we used elevation as proxy for environment (highly correlated with most bioclimatic variables, see supplementary information in Hopping et al. (2018) and tested for IBE by measuring the Mantel correlation between population pairwise F_{ST} and elevational differences.

We conducted three different analyses to investigate the genetic structure of *T. shambalaensis* (Figure 1c, Figure 2). First, we conducted a discriminant analysis of principal components (DAPC) to determine the most likely number of genetic clusters without prior knowledge of the geographical location of each sample (Jombart et al., 2010; implemented in R package adegenet, Jombart, 2008). We iterated from 1 to 20 clusters and selected the number of genetic clusters with the lowest Bayesian Information Criterion (BIC) score. We visualized the selected clustering result in a principle component analysis (PCA) for SNP data (Patterson et al., 2006). Multivariate approaches to clustering such as DAPC make no assumptions about ancestral populations. Secondly, we estimated the ancestry coefficients of each individual using sparse non-negative matrix factorization algorithms (sNMF, Frichot et al., 2014, implemented in the LEA package in R: Frichot & François, 2015), which is a likelihood-based approach to investigating ancestry proportions. We iterated over *K*-values from 1 to 20, each with 10 replicate runs, and selected the *K*-value with the lowest cross-entropy score, which indicated lowest error in assigning number of supported ancestry (Frichot et al., 2014.). Finally, we visualized all individuals on a phylogenetic network generated by the neighbour-net algorithm (Bryant & Moulton, 2004, implemented in SPLITSTREE version 4.16.1 Huson & Bryant, 2006).

We estimated historical relationships among the seven valley populations using TREEMIX (v1.12, Pickrell & Pritchard, 2012). We generated 1000 bootstrap replicates, each with a 1000-SNP resampling block. We first estimated the maximum likelihood phylogeny without allowing for migration or admixture, then sequentially added migration events to test whether any of these significantly improved the likelihood fit. The *p*-value for the added weight of migration edges is derived from jackknife estimates (but see discussion in Pickrell & Pritchard, 2012).

2.3 | Modelling historical gene flow

To understand the historical process that generated contemporary genetic structure of *T. shambalaensis* populations, we conducted coalescent simulations using FASTSIMCOAL2 (v 2.6.0.2, Excoffier et al., 2013) to compare the composite likelihood for each population's site frequency spectrum (SFS) under different dispersal scenarios. Specifically, we generated different sets of dispersal distance matrices among populations (see descriptions below), and used the distances among populations to constrain the proportion of symmetrical migrants allowed between populations at each generation in coalescence. In each simulation, the seven populations were

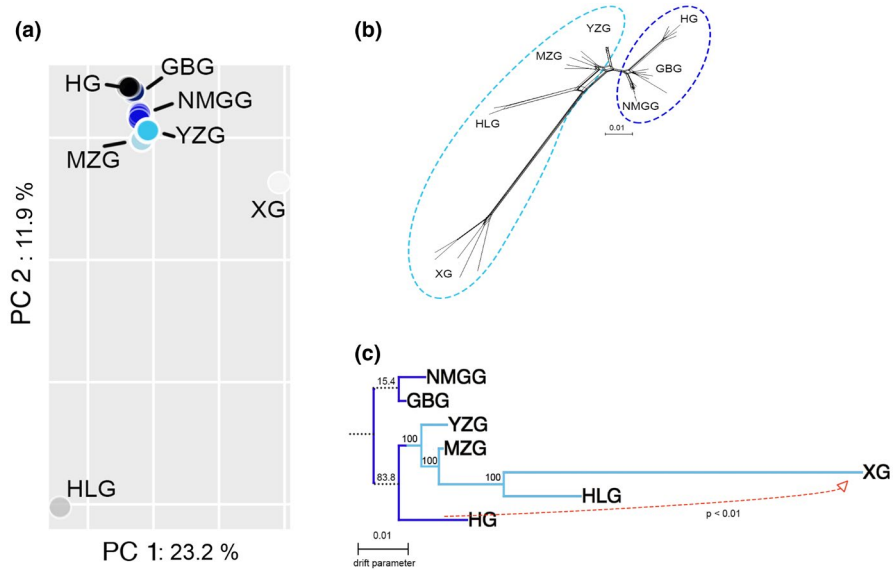

FIGURE 2 Population structure of *T. shambalaensis* in seven glacier valleys on the eastern slope of Mt. Gongga, China. (a) First two PCs from DAPC analysis. Each individual is represented by a single dot. Individuals from the same valley are assigned the same colour. Since intrapopulation differentiation is small, individuals within the same populations show up as overlapping dots. (b) Neighbour-net visualization of phylogenetic network. A maximum of 5 random individuals per population were presented here to reduce graphical complexity. Dotted circles showed the northern (dark blue) and southern (light blue) populations. (c) Maximum likelihood tree from TREEMIX, with support from 1000 bootstraps labelled. Low support nodes are connected by dashed lines. Dotted red line indicates one potential migration edge detected from jackknife estimates of added edge weight

allowed to migrate symmetrically with each other, but the number of migrants between populations was proportional to the inverse of their "distances". This was achieved through setting up a migration matrix in each FASTSIMCOAL2 template file with migration rates as parameters (see *.tpl files in Supplementary material), and constraining these parameters in the "complex parameter" setting of the FASTSIMCOAL2 range file (see *.est files in Supplementary material). In other words, each set of distance matrices tests a different hypothesis about intrapopulation migrations. We assumed a simple "island model" in which gene flow between populations (represented by number of migrants), is correlated with the inverse of "distance" (Wright, 1931; Rottenstreich et al., 2007; but for some empirical qualifications see Whitlock & McCauley, 1999). Sets of distance matrices aimed at modelling the fine-scale historical, geographical and environmental changes of the landscape are:

2.3.1 | Glaciation history

We traced the dated moraine distribution of Mt. Gongga (Wang, Pan, et al., 2013) onto a 1:10 m elevation map from NATURAL EARTH (www.naturalearthdata.com). Known moraine distributions represent the maximum extent of ice sheet coverage during (1) little ice age (LIA, ~2 kya), (2) neoglaciation (~12 kya), (3) marine oxygen isotope stage 2 (MIS2, ~29 kya, also referred to as the global last glacial maximum LGM), (4) early MIS3 (~35 kya) and (5) mid-MIS3 (~58 kya, also labelled as local last glacial maximum LGM_L, summarized in Table 2a). Current population distributions are represented as dots on a 840 × 600 raster. We extrapolated the historical distribution of each population from its current location: post-LGM_L glacial retreat carved out the existing drainage terrain at Mt. Gongga, so we assumed that each surviving population has persisted in the periglacial refugia cut by the receding glacier valley river. We further assumed that these populations did not move across the flanking mountains. Figure 3a shows how this was simulated backward in time, where the locations of historical populations were represented as a few pixels on map, being deposited along the river valleys as the glacier "advanced". We first calculated six sets of Euclidean distances between populations (one on the modern landscape, as well as five historical landscapes, see Figure 3b "Euclidean distance"). We then assumed that glaciers are impermeable barriers to gene flow and calculated the shortest distances (hence referred to as 2D "least cost" path) between populations (Figure 3b "avoid glaciers").

2.3.2 | Habitat range

Since *T. shambalaensis* is endemic to the valleys of Mt. Gongga and the habitats of different populations are similar in elevation and climate, ecological niche modelling (ENM) of past and present distributions is difficult. However, since all known high-elevation *Thitarodes* species have been recorded to occur only in caterpillar fungus habitat (Wang & Yao, 2011), we assume that the habitat conditions of locations where caterpillar fungus is documented to occur provides a reliable proxy of the environment inhabited by *Thitarodes* moths on their own. Earlier research has shown that among all caterpillar fungi in the Himalayan-Hengduan region, elevation (3600–4600 m) and mean temperature of the coldest quarter (−10 to −4°C) are the best predictors of existing habitat (Hopping et al., 2018). These elevational and temperature ranges cover all known *Thitarodes* lineages and represent a broad environmental range a single population could adapt to. Thus in one set of distance matrices, we modelled these elevation or temperature ranges as the only conditions in which gene flow is allowed. First, on the modern landscape (elevation data from NATURAL EARTH, 30 arc sec climate data from WORLDCLIM, Fick & Hijmans, 2017), we calculated the shortest distances between populations within the specified elevation and temperature ranges (Figure 3b "range restriction"). We then applied the temperature range restriction on the moraine-inferred population distribution during MIS2, using the 30 arc sec paleoclimate data of LGM (Karger et al., 2017). We did not apply the current elevational range to restrict the distribution of MIS2 populations. On both current distribution and MIS2 distribution maps, we further imposed the rule that existing glaciers are impermeable gene flow barriers and calculated another set of population distances within the specified elevation or temperature ranges.

2.3.3 | Isolation by resistance

A potentially more accurate way to model the effect of environment on gene flow is to consider the environmental "resistance landscape" to gene flow (McRae et al., 2008). Since all climate variables that predict the habitat of caterpillar fungi are highly correlated with elevation (Hopping et al., 2018), we used change in elevation along the "dispersal paths" as a proxy for environmental resistance: (1) In a first set of distance calculations, "dispersal paths" were the 2D "least cost" path derived in the previous section ("*Glaciation history*"), but we integrated the total distances traversed as if these paths were projected onto a 3D plane with elevational data. Compared with 2D Euclidean distances between habitats, this new measurement imposes much higher costs for individuals directly crossing the high mountains separating neighbouring cul de sac habitats. (2) In a second set of distances, we applied Dijkstra's algorithm (Dijkstra, 1959) in circuit theory to find "least resistance paths" between populations on a 3D plane. We modelled the "resistance" to gene flow as the inverse of the absolute difference in elevation between two adjacent cells in our 840 × 600 raster (i.e., symmetrically higher resistance for making bigger "jumps" to higher or lower elevations), and calculated the path connecting populations with the least amount of total "friction" (for details see van Etten & Hijmans, 2010, implemented in package gdistance in R: van Etten, 2017). The resultant path minimizes the change in elevation during dispersal events from one population to another (Figure 3b "least elevation transit"). If previous approaches of drawing straight lines between populations (on

TABLE 2 (a) Time periods used in coalescent models. (b) Historical models of environmental resistance in gene flow between populations, ranked by their coalescent simulation likelihood

(a)

Time period	Model label	Moraine dating	Events
Little ice age	LIA	~2 kya	
Neoglaciation	Neoglacial	~12 kya	
Marine Isotope Stage 2	MIS2	~29 kya	Global last glacial maximum LGM
Early-Marine Isotope Stage 3	MIS3	~35 kya	
Mid-Marine Isotope Stage 3	LGM_L	~58 kya	Local last glacial maximum LGM_L

(b)

Model	Time period	Habitat restrictions	Path finding	Distance calculation	Mantel R	AIC (mean)	AIC (min)	Δ AIC
25	LGM_L	Glacier	Least cost	3D distance	0.48	59702	59667	0
41	LGM_L	Glacier	Least resistance	3D distance	0.59	59718	59690	22
38	MIS3	Glacier	Least resistance	2D distance	0.62	59806	59782	114
37	MIS3	Glacier	Least resistance	3D distance + climate distance	0.62	59846	59819	152
26	MIS3	Glacier	Least cost	3D distance	0.52	59870	59844	176
42	MIS3	Glacier	Least resistance	3D distance	0.58	59914	59879	212
9	Neoglacial	Glacier	Least cost	2D distance	0.60	59928	59896	229
24	LGM_L	Glacier	Least cost	3D distance + climate distance	0.52	59936	59898	231
23	MIS3	Glacier	Least cost	3D distance + climate distance	0.58	59941	59910	243
10	MIS2	Glacier	Least cost	2D distance	0.53	60029	59981	313
39	LGM_L	Glacier	Least resistance	3D distance + climate distance	0.58	60069	60031	363
40	LGM_L	Glacier	Least resistance	2D distance	0.58	60196	60166	499
6	LGM_L		Euclidean	2D distance	0.45	60439	60375	707
5	MIS3		Euclidean	2D distance	0.56	60511	60475	808

Note: Only the 15 most likely models are shown here. See Table S4 for full table. Model details can be found according to model numbers in the Supplementary material. Each model is specified by the "time periods" for which the population location is inferred (from modern to LGM_L), which habitat range is applied to allow for gene flow (climatic or elevational range), and whether or not glaciers are set as impermeable barriers to gene flow. Paths in each model were found by Euclidean distance, shortest path ("least cost") or calculating "least resistance" path in circuit theory. The established paths were traced and tallied either on 2D plane or 3D (accounting for distance moving up and down the elevation), and the BEDASSLE coefficient can be added to account for contribution of environment to genetic divergence. We calculated the Mantel R of each set of distances with pairwise population F_{ST}. Each model was run independently 100 times in FASTSIMCOAL2, and we show the mean and minimum AIC value of each model. All models have the same number of parameters (50).

either 2D or 3D planes) represent distances "as the crow flies", then resistance distances are more commonly characterized as distances "as the wolf runs" (van Etten, 2017). This approach more realistically models individuals avoiding geographical barriers during their dispersal. For comparing models of distance calculation between 2D and 3D planes, these resistance distances (generated in 3D) were also projected down to 2D (called "least resistance path 2D" in Figure 3d). All path calculations were repeated on six (contemporary and historical) landscapes, with glaciers modelled as impermeable barriers to gene flow.

2.3.4 | Environmental contribution to divergence

The above-mentioned models predict paths (of “least cost” or “least resistance”) by which the populations would disperse across a topologically complex landscape but do not quantify the effect of environmental variance on divergence. High mountains and low valleys are stronger barriers to gene flow than a flat landscape not only because of extended topological dispersal distance, but also because organisms are not well-adapted to the environmental range traversed (Ghalambor, 2006; Janzen, 1967). We thus used Bayesian estimation of differentiation in alleles by spatial structure and local ecology (BEDASSLE, Bradburd et al., 2013) to quantify the contribution of geographic and environmental isolation on genome-wide differentiation between our populations. Following the model formulation of Bradburd et al. (2013) that specified the effect size of both the geographic matrix (pair-wise Euclidean distance) and the environmental matrix (in our case, pair-wise elevational differences), labelled as α_D, and α_E, we conducted 1,000,000 Markov chain Monte Carlo (MCMC) simulations using the BEDASSLE (Bradburd et al., 2013) package in R. After a

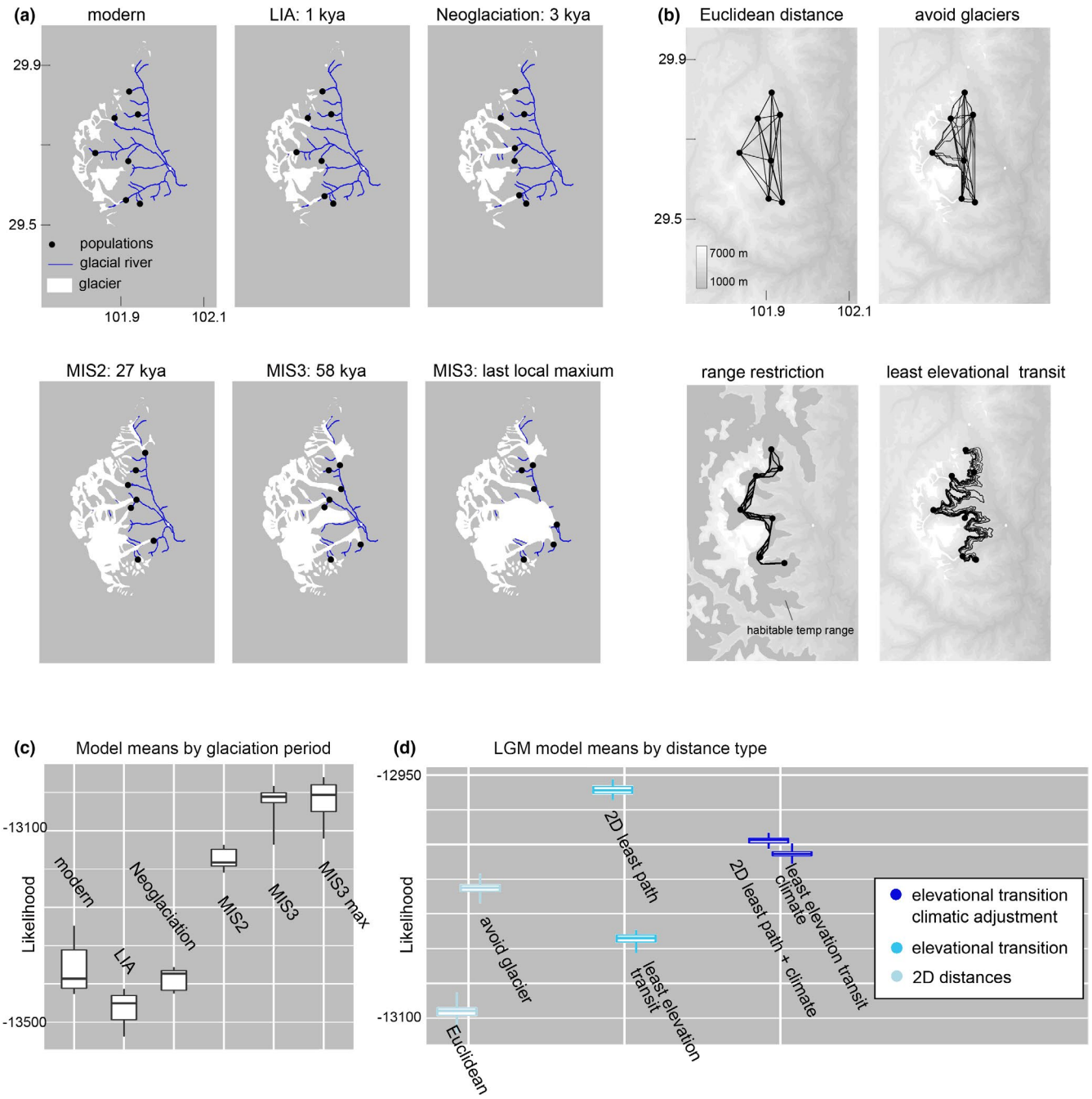

FIGURE 3 Models of historical gene flow and environmental resistance. Panels in (a) and (b) show the glaciers of Mt. Gongga and encompass the same geographical extent as Figure 1b, with the *y*-axis indicating latitude. (a) Models of historical population locations based on the assumption of periglacial colonization, from modern day to last local maximum. Extent of historical ice sheets are traced from dated moraine data of Wang, Pan, et al. (2013). The glacier rivers (blue lines) are traced from current water flows. (b) Example of sets of relative distances between populations, between population location: Euclidean distances, "least cost path" that avoids crossing over glaciers, "least cost path" within suitable habitat range (mean temperature of the coldest quarter −10 to −4°C) labelled in grey and "path of least resistance" that minimizes total change in elevation between paths connecting two populations. (c) Mean FASTSIMCOAL2 simulation maximum likelihood estimates for models based on different glaciation periods (all models have the same number of parameters). Bar indicates the mid-50 percentile of the 100 independent runs. Models higher on the *y*-axis are more likely given the observed data. (d) Mean FASTSIMCOAL2 simulation maximum likelihood estimates for LGM models by distance type, representing a subset of "MIS3 max" shown in (c). Models are shown as three separate categories of paths: those that consider landscape as flat (light turquoise), as 3D (light blue) and as 3D with environmental contribution to genetic divergence (dark blue). Models higher on the *y*-axis are more likely given the observed data

50% burnin, we sampled parameter values every 100 generations and evaluated model convergence using the built-in graphic functions in BEDASSLE (see Supplementary material for setting of priors on mutation steps). We obtained a "conversion coefficient" (α_E/α_D) to convert the effect on genomic divergence of elevational traverse during dispersal into equivalent geographical distances.

In these set of models, we followed the "least cost paths" and "least resistance paths" previously calculated on the 3D landscape, but we applied an extra distance of environmental change to account for accumulated change in elevation in the path (e.g., $D_{new} = D_{least\_cost} + D_{elevation}\ (\alpha_E/\alpha_D)$).

All sets of distance matrices generated are presented in Table 2b (also see Supplementary material). Prior to coalescent simulations, we also applied Mantel tests (Mantel, 1967) to check whether any of these new distance matrices differed significantly from the matrix of Euclidean distances between contemporary populations (that is, the one we used to assess IBD). We also applied the same tests for correlation between population pairwise F_{ST} and these new distance matrices.

We used the above-mentioned sets of distance matrices as constraints on migration rate in FASTSIMCOAL2 simulations. When computing the observed joint site frequency spectra (SFS) of all populations (used as input for FASTSIMCOAL2), we projected the full data matrix down to no more than six samples per population to account for missing values and reduce computational complexity (Marth et al., 2004, implemented in easySFS script in: https://github.com/isaacovercast/easySFS/issues/5). Each of our coalescent runs had the following specifications: each population started with prior effective population size ~uniform (U) (10 k, 1 million) and mutation rate of 2.5×10^{-8} per generation (a parameter whose value falls between that estimated for Lepidoptera in Keightley et al. (2015) and that estimated for Orthoptera in Ney et al., 2018). For each run, 100,000 (-N) coalescent simulations were conducted, with 40 expectation-maximization cycles (-L) and threshold for observed SFS entry count set as 10 (-c). We conducted 100 independent FASTSIMCOAL2 runs per model to determine the simulation with maximum composite likelihood (see Supplementary material for settings).

2.4 | Modelling divergence

To estimate the timing of migration and population expansions, we modelled the demographic histories among the four populations that were historically under the same extended ice sheet in this region (YZG, HLG, XG, MZG). We modelled their lineage history following the ML phylogeny from TREEMIX (populations coalesce sequentially at time T_{HX}, T_{MX}, T_{YX} in Figure 4), and posited a resizing (expansion or contraction) event for each population at time T_{Exp}. We compared the likelihood of two models: one in which populations exchanged migrants prior to resizing ("pre-expansion migration model" or "historical migration model"); another in which migration occurred following population resizing ("post-expansion migration model" or "contemporary migration model"). We selected projections per population that maximized the number of segregating sites to compute observed joint SFS of all populations. The parameters for these simulations were the same as those used in 2.3. After 100 independent FASTSIMCOAL2 runs per model to select parameters from the model with the maximum composite likelihood, we also conducted 100 bootstraps, each taking random 100-SNP blocks and repeating the analysis to obtain confidence intervals (see Supplementary material for settings).

To cross-validate patterns of demographic resizing obtained from FASTSIMCOAL2 simulations, we used *δaδi* (version 1.7.0, Gutenkunst et al., 2009) to model the historical population changes from each

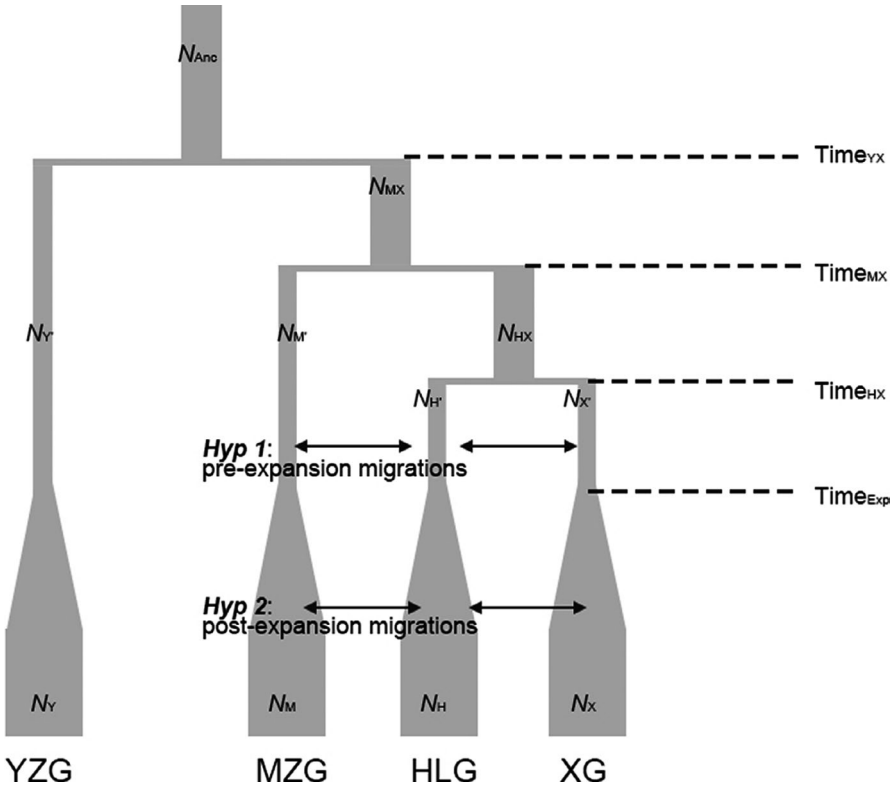

FIGURE 4 Comparison of historical and contemporary FASTSIMCOAL2 models of migration among 4 populations under the same historical ice sheet. Tree topology followed the ML tree of TREEMIX. Each branching event (at time T_{HX}, T_{MX}, T_{YX}) is modelled as population coalescence with a resizing event. Coalescence, backward from present to historical time, is shown from bottom to top. We also posited a recent resizing event at T_{Exp} for each population. In the pre-expansion (historical) migration model (horizontal arrows indicated in "Hyp 1"), populations were allowed to migrate between T_{Exp} and T_{HX}. In the post-expansion (contemporary) migration model (horizontal arrows indicated in "Hyp 2"), populations were allowed to migrate from present to T_{Exp}

population's one dimensional SFS. For each population we tested the likelihood of 4 models: (1) constant population size; (2) constant population size followed by constant growth or retraction; (3) constant population size followed by exponential growth or retraction; (4) constant population size followed by instantaneous decline followed by growth or retraction (bottleneck). Models (2) and (3) would be expected for populations affected by glaciation. We performed 3 rounds of optimization following Portik et al. (2017) and used Godambe Information Matrix (GIM, Coffman et al., 2016) to compare maximum likelihood models. We conducted 100 replicate simulations per model.

2.5 | Single valley analysis

To test whether subpopulation genetic structure is distinguishable within a single valley population, we repeated our DAPC (Jombart et al., 2010), sNMF (Frichot et al., 2014) and neighbour-net (Bryant & Moulton, 2004) analysis on 30 individuals collected within the YZG valley, which we selected for more detailed substructure analysis because it includes an accessible main glacier and a river that melts from a northern glacier. Our samples belonged to 5 localities within the YZG valley on different sides of the glacier and rivers (Figure 5a, Table S1).

We could not construct an ML phylogeny at the subpopulation level due to a lack of sufficient genetic differentiation. Instead, we used FASTSIMCOAL2 and modelled six different scenarios of subpopulation history involving glaciers changes (see Table S3). The observed joint SFS of all subpopulations were calculated using the number of projections that maximizes the number of segregating sites in each subpopulation. Since our aim was to select the best model for lineage divergence history, we did not allow cross-subpopulation migration in any of the models, and all parameters were specified the same as in 2.3 and 2.4. These settings would probably increase the estimate for coalescence time, but were unlikely to affect the lineage topology of the most likely model. For each model, we conducted 150 independent runs to determine the simulation with maximum composite likelihood (see Supplementary material for settings).

3 | RESULTS

3.1 | Sequencing and SNP-calling

After quality-filtering, we obtained on average 6.5 million reads per sample ($n = 122$, SD = 2.1 million; sample information see Table S2). A total of 23 samples (19%), mostly from GBG valley, shared only a negligible number of enzymatic cut sites with *T. shambalaensis* (Figure S1) and did not form a monophyletic group with *T. shambalaensis* in the CO1 phylogeny (see Wang, Zhuang, et al., 2019). These belong to an undescribed *Thitarodes* species only distantly related to *T. shambalaensis*), and were not included in our analysis. After filtering the SNP catalogue generated by CSTACKS, selecting loci with less than 10% missing data across all individuals, we obtained a total of 11,038 SNPs across 2373 loci. One SNP per locus was randomly selected. Our final data set contained 2373 SNPs from 99 individuals, with 7.09% missing data (see Table 1 for post-filtering sample counts, see Figure S2 for STACKS parameter sensitivity, see Supplementary material for final SNP matrix).

3.2 | Population structure and phylogeny

With distance measured as Euclidean distances, population pairwise F_{ST} showed a significant signal of IBD (Mantel $p = .03$, $r = .52$, Figure S3A). With environmental distances measured as population elevational differences, we did not detect a signal of IBE (Mantel $p = .56$, $r = -.02$, Figure S3B). Population statistics were summarized in Table 1. Although F_{IS} per population was high (mean = .17, SD = 0.05) and H_{obs} was lower than H_{exp} (mean difference = 0.03), we did not detect any loci that significantly deviated from HWE ($p = 1.00$ after Bonferroni correction). The genetic diversity (H_{obs} and π) and F_{IS} of each population had no significant correlation with geographical coordinates, elevation or sample size (multiple regressions, $p_{\pi} = 0.39$, $p_{Hobs} = 0.37$, $p_{F} = 0.13$, Figure S4).

DAPC analysis found the lowest BIC scores for 7 genetic clusters ($k = 7$) among the 99 individuals, with each genetic cluster corresponding to the valley where the sample was collected (Figure S5A), although values of k between 5 and 9 all had low BIC scores. In our principal component visualization of genetic differentiation, the first PC accounted for 23.2% of the total variation and identified samples from the two southern-most valleys (XG and HLG) as different from the rest of the samples, while the second PC accounted for 11.9% of the total variation and separated samples by latitude (Figure 2a). Estimation of the ancestry coefficients using sNMF found the highest support for six genetic clusters (Figure S5B, $k = 6$, while values of k between 5 and 7 all had low cross-entropy scores), with each valley population corresponding to its own genetic cluster except the GBG samples, which were a mixture of populations from the valleys to the north (HG) and south (NMGG, YZG) (Figure 1c). Network representation by neighbour-net algorithms showed that all southern valleys that shared the same historical ice sheet (YZG, MZG, HLG, XG) formed a single cluster (Figure 2b). Furthermore, the ML phylogeny from TREEMIX supported the monophyly of the southern populations (100% bootstrap support), while the relationship between the monophyletic lineage and other populations were not well resolved (Figure 2c). Postulating a migration event close to the branch tip of HG to XG significantly increased the likelihood of the TREEMIX model.

3.3 | Modelling the landscape of historical gene flow

We generated 47 sets of distance matrices between populations to account for historical landscapes and environmental resistance

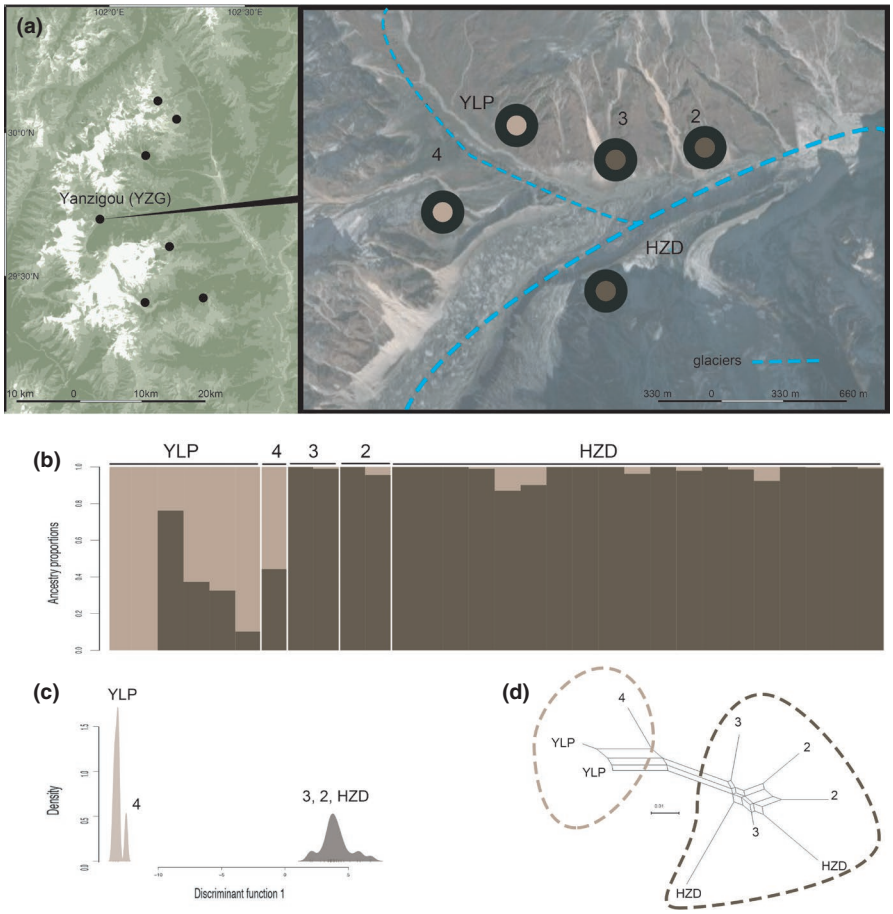

FIGURE 5 Subpopulation structure of *T. shambalaensis* inside the Yanzigou valley, Mt. Gongga. (a) Subpopulation location within YZG. The samples were collected from Haizidang (HZD), Yangliuping (YLP) and unnamed locations 2, 3, 4. The thicker blue dashed lines indicate the main YZG glacier; the thinner blue dashed line indicates the drainage from another northern glacier. Dot colour corresponds to the genetic cluster the subpopulation is assigned to in DAPC. (b) Results of sNMF analysis for best fit $K = 2$. Each bar is an individual ($n = 30$); two colours represent admixture of genetic clusters. (c) Density of the first DAPC discriminant function separates samples into two genetic clusters. (d) Neighbour-net visualization of phylogenetic network among subpopulations. A maximum of two individuals per subpopulation are presented to reduce graphical complexity. The topology of the full data set does not maintain the monophyly of YLP samples since both YLP and location 4 have detectable admixture; samples from the two dashed circle clusters remain distinct from each other in the full data set

to gene flow (Table 2b). Most of these distance sets are minor modifications of, and thus highly correlated with, the contemporary Euclidean distances (Figures S6 and S7). In reconstructing the historical position of populations from moraine records, the relative distance between YZG and MZG populations, as well as that between HG and GBG populations increased since MIS3, while the relative distance between XG and HLG have decreased (Figure 3a). The absolute distances across all populations increased from postulated LGM_L localities to contemporary localities by 36% (SD = 0. 27, Figure S8). Our BEDASSLE simulations reached a "conversion coefficient" (α_E/α_D) of 1.4 (i.e., each 1 m change in elevation of *T. shambalaensis* habitat amounts to 1.4 m of geographical isolation in terms of its contribution to genetic variation, Figure S9). The strengths of IBD correlations (measured as Mantel r statistics, McRae & Beier, 2007) in historical models were significantly greater than those in contemporary distance models ($t = 5.17$, df = 26, $p < .01$); the strengths of IBD correlations in models based on least resistance paths were significantly greater than those in models based on Euclidean distances ($t = -2.52$, df = 35, $p = .02$).

Four models failed to coalesce in our FASTSIMCOAL2 simulations (Table S4, Figure S10); these are models in which gene flow was limited to an elevational range or climate range, while setting glaciers as impermeable barriers of dispersal completely blocked paths between populations. All models have the same number of parameters (50). Among the 44 models that coalesced, those that based their distances on MIS2, MIS3 and LGM_L population distributions had significantly higher likelihood than their modern and Holocene counterparts (Figure 3c; $t = -6.29$, df = 41.41, $p < .01$). The most likely models were based on the population locations of LGM_L (Table 2b). Among models that used the population distribution of LGM_L, those that were based on Euclidean distances had the lowest likelihoods, significantly outcompeted by ones with the more realistic consideration of environmental resistance, such as avoiding glaciers, or

taking into account elevation transition and/or climate transition (Figure 3d; $t = 74.04$, df = 700.55, p-value < .01).

3.4 | Modelling divergence

Between the pre and post-expansion migration models of monophyletic populations of YZG, HLG, XG and MZG, we found greater support that migration among the populations happened before population resizing (Table S5). The most likely model placed the start of population resizing at 41 k generations ago (95% CI: 34–42 k, Table 3a). Assuming a 1–1.5 year generation time for *Thitarodes* (Tao et al., 2016), this places the timing of likely among-population migrations during LGM_L, which is consistent with our result that most likely models of historical and environmental resistance of gene flow are based on the population location of LGM_L.

Our FASTSIMCOAL2 models suggest that with the exception of XG (whose population remained almost constant), the post-LGM_L population experienced a 30- to 100-fold expansion (Table 3a). Similarly, 1D SFS simulations of each population from $\delta a \delta i$ suggested that, with the exception of HLG, which showed population decline, scenarios of "constant growth" and "exponential growth" (4–20 fold expansion) are most likely for all populations (Table 3b, model selection see Table S6).

3.5 | Single valley

Among 30 individuals in five different localities within YZG, both DAPC and sNMF analysis found greatest support for two genetic clusters (Figure 5b,c, Figure S11). Individuals adjoining the northern glacial river (from locality 4 and YLP) form one genetic cluster, while individuals on both sides of the main glacier (HZD south of the main glacier, and habitat 2, 3 north of the main glacier) form another genetic cluster. This clustering is consistent with the phylogenetic network of neighbour-net, which separated the two clusters by their glacier association (Figure 5d).

Among six FASTSIMCOAL2 models of different subpopulation histories, we obtained greatest support for a lineage history in which subpopulations in YLP and location 4 are sister to the monophyletic cluster of HZD, location 3 and location 2 (Figure S12, Table S3). The hypothesized tree topology was based on the scenario in which an ancestral population near the periglacial refugia diverged into a subpopulation at locality 4 and YLP as the norther glacier cut into the valley. Later, in smaller glacier cycles in which the YZG main glacier advanced, HZD was physically separated from locality 2 and 3 (Figure 6).

4 | DISCUSSION

Our results uncovered genome-wide signatures of late Pleistocene glaciation on the population structure of *T. shambalaensis* on the eastern slopes of Mt. Gongga. Specifically, (1) the results of valley-based genetic clustering and a signal of IBD among populations supported the hypothesis that the topology of mountains flanking parallel valleys are effective barriers to gene flow. (2) Correspondence between population (and subpopulation) lineage history and the history of glacial retreat supported the hypothesis that population divergence followed the formation of valleys carved out by retreating ice sheets. (3) Modelling of the historical landscape supported the hypothesis that historical populations migrated during LGM_L, followed by relatively isolated population expansion post-LGM_L. Since many of our historical inferences are model-based, we applied different methods of inference to verify that our results are robust even when subjected to specific model parameter choices. By observing which results hold up across different models, we can be more confident about the validity of our historical inference. We discuss each of our findings and their implications below.

4.1 | Fine-scale population structure and IBD

Thitarodes shambalaensis populations in this study come from parallel glacier valleys no more than 10 km apart, but we were still able to select for 6–7 well-supported genetic clusters that correspond to each population's geographical distribution as our most likely hypothesis of population structure. In other words, variation exhibited by 2300 SNPs was sufficient to trace each individual to its habitat. While genetic structure of populations within 10 km has been reported in plants (Geng et al., 2009; Helsen et al., 2015; Hevroy et al., 2018; Kitamura et al., 2018), amphibians (Kobayashi et al., 2018), reptiles (Pearson et al., 2020), fish (Ciannelli et al., 2010) and mammals (Ziege et al., 2020), fine-scale genetic structure for flying insects is rare. For example, a similar number of SNPs used to study ants (Boyle et al., 2019; Smith et al., 2019), beetles (Weng et al., 2021) and butterflies (MacDonald et al., 2020) identified meaningful genetic clusters between long-distance populations that reflect their geographical isolation, but in these studies, populations within 10 km of each other were genetically hard to distinguish. Factors intrinsic to *Thitarodes* biology, as well as external geographical factors, contributed to the maintenance of genetic structure in geographically adjacent populations that are often characteristics of low-vagility, short-range endemic terrestrial arthropods (e.g., Peres et al., 2018; Schwentner & Giribet, 2018). For example, fungi-associated *Thitarodes* are known to have unusually strict habitat requirements (Hopping et al., 2018; Wang et al., 2020) and low adult dispersal due to their short period of activity (Maczey et al., 2010; Zou et al., 2011). In terms of their abiotic environment, the valleys of Mt. Gongga are famously deep and topologically complex, and a 10 km separation by Euclidean distance between populations may represent a much longer distance in the context of gene flow.

We detected a clear signal of IBD (pairwise F_{ST} vs. Euclidean distance) among the seven genetically distinct populations, but no signal of IBE (pairwise F_{ST} vs. elevational distance). This allows us

TABLE 3 (a) Inferred parameters and confidence interval for preresizing migration FASTSIMCOAL2 model in Figure 3

(a)			
		95% CI	
Parameters	**Point estimates**	**Lower bound**	**Upper bound**
T_{Exp}	41,684 generations	34,074	41,911
T_{HX}	45,385 generations	36,088	45,468
T_{MX}	53,691 generations	50,044	54,074
T_{YX}	60,024 generations	57,756	60,960
Res_{XG}	1.04 (near constant)	0.66	1.66
Res_{HLG}	0.03 (expansion)	0.01	2.74
Res_{MZG}	0.01 (expansion)	0.00	0.01
Res_{YZG}	0.01 (expansion)	0.00	0.01

(b)				
			95% CI	
	Best model	**Expansion**	**Lower bound**	**Upper bound**
HG	Exponential growth	20.66	11.74	99.33
GBG	Constant growth	5.54	5.45	5.78
NMGG	Exponential growth	7.26	5.65	7.27
YZG	Exponential growth	31.88	29.52	33.02
MZG	Constant growth	8.48	7.93	8.77
XG	Constant growth	4.07	3.95	4.58
HLG	Constant decline	0.01	0.01	0.01

Note: Point estimates were taken from the minimum AIC model out of 100 independent runs. Confidence intervals were taken from the minimum AIC model from each of the 100 bootstrap runs (each with 100 independent runs with 100 SNPs). Time estimates are in number of generations. Resizing parameter values between 0–1 suggest recent population expansion, while >1 suggests population decline. (b) Best demographic model for each population inferred from $\delta a \delta i$. Confidence interval from 100 replicate simulations. Best model is selected from models of (1) constant population size; (2) constant growth or retraction; (3) exponential growth or decline; (4) instantaneous decline followed by growth or retraction (see Table S6 for model selection). Expansion coefficients >1 suggest population growth is either constant or exponentially increasing

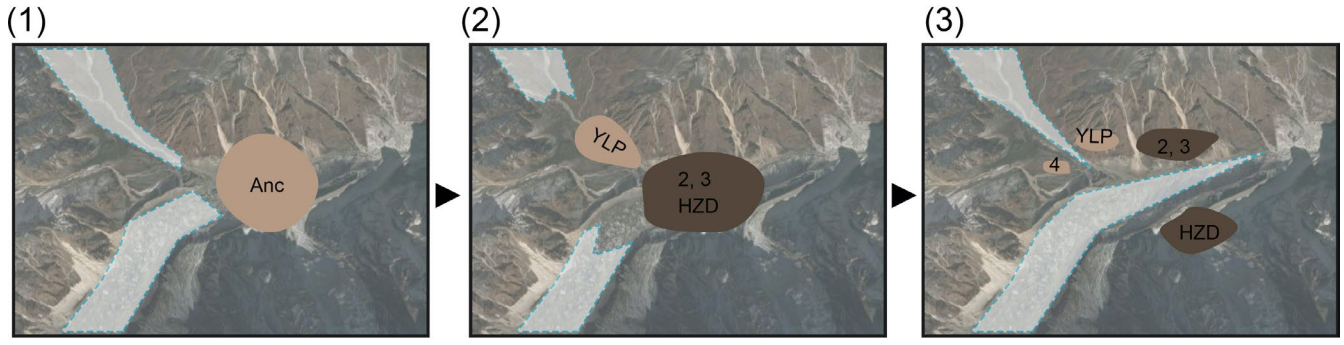

FIGURE 6 Historical interpretation of the most likely model of the lineage history of *T. shambalaensis* subpopulations inside Yanzigou valley. Glacier shown in white shading. (a) An ancestral population (Anc) resided near a periglacial refugium, (b) it then diverged into a subpopulation (YLP) as the northern glacier cuts into the valley. (c) Subsequent advancement of YZG main glacier physically separated subpopulations on two sides of the glacier

to apply landscape-derived distance matrices to further probe the historical mechanics of genetic differentiation (see Section 4.3). The emergence of an IBD pattern is highly dependent on the scale of landscape taken into consideration (van Strien et al., 2015). Central to the IBD process is the assumption that gene flow is proportionally inversely affected by the distance between populations. At a small geographical scale, the signal of geographical isolation is often overwhelmed by more immediate, sometimes anthropogenic, environmental differences such as a rural-to-urban gradient (Ziege et al., 2020) or cohort characteristics (Kitamura et al., 2018; Pearson et al., 2020). Signals of IBD at a fine scale are often weak (Crookes & Shaw, 2016; Hevroy et al., 2018), or otherwise nonexistent. Our

detection of IBD suggests that among *Thitarodes* populations, even at close physical proximity, landscape is still a prominent barrier to gene flow. Admittedly, our experimental design was better able to detect IBD than IBE: the seven populations sampled have relatively small differences in terms of their environments (a maximum of only 200 m difference in elevation) and selectively neutral SNPs derived from RADseq are not well-suited for picking up signals of adaptation to environmental differences (Orsini et al., 2013). Furthermore, in modelling environmental resistance we assumed that upward and downward elevational deviations from current population ranges symmetrically impedes geneflow, while the minimum and maximum critical thermal tolerance of *T. shambalaensis* might be asymmetric. To detect population-level adaptation of this *Thitarodes* system, additional research focused on assessing molecular markers under selection, incorporating data from physiology measurements, and taking into account differences of each population's strain of parasitic fungi as a component of "environmental" difference would be necessary.

4.2 | Glaciation and lineage history

While each population was isolated by its dispersal limits, our results also revealed a signature of glaciation history on population divergence. Specifically, our ML phylogeny found samples from the southern valleys of YZG, MZG, XG and HLG to be monophyletic. Since these valleys were carved out from the retreat of a single large ice sheet post-LGM_L (and still share the same drainage system west of the Moxi river, Figure 1b), the monophyly of the four lineages suggest that a single ancestral population diverged into four populations as the receding ice-sheet carved out four parallel valleys. This is not the case for samples from the northern valleys (HG, GBG, NMGG). The formation of these northern valleys each resulted from an individual ice sheet retreat, and we found no signal of monophyly between populations in the northern valleys. We note that one way to provide further evidence that ancestral periglacial species diverged into the four southern valleys is to look for phylogeographic concordance among other species co-distributed with *T. shambalaensis*, which would suggest a convergence in response to topographic history (Marske et al., 2020; Thomaz & Knowles, 2020). We expect populations of high elevation *Rhododendron* or *Pedicularis* plants that also occur at *T. shambalaensis* habitats in all seven valleys of eastern Mt. Gongga will exhibit similar patterns of monophyly in the southern 4 valleys.

In our study, the pattern of lineage history recapitulating the history of glacial retreat reaches its extreme when examining the subpopulation structure of individuals within YZG valley. At the current glacier tongue of YZG (Figure 5a), we examined samples divided by the main YZG glacier and a smaller ravine flowing from a northern glacier. Results of our genetic clustering showed that samples on both banks of the YZG main glacier form an indistinguishable genetic cluster, while samples on both banks of the northern ravine form a separate genetic cluster. In other words, individuals at location 3 are almost genetically identical to samples from HZD on the other side of the glacier, while they are distinct from YLP individuals on the same side of the mountain range (Figure 5). This pattern cannot be satisfactorily explained by any measure of dispersal limitation across the subpopulations: it is difficult to posit migration across a 500 m wide glacier between location 3 and HZD while having no gene flow across homogenous habitat from location 4 to YLP. The most parsimonious explanation for the observed genetic clusters is to take into account historical divergence of subpopulations at the edge of retreating glacier tongues. We hypothesize that all subpopulations shared a periglacial ancestral population when the YGL glacier initially retreated near its contemporary location (Figure 6a). A subpopulation diverged from the ancestral population when the northern glaciers retreated and left open more space for colonization at the northwest edge of the YZG glacier. This formed the ancestral population for YLP and location 4 (Figure 6b). All contemporary geographical separation between location 4 and YLP, or between location 2, 3 and HZD, happened relatively recently after the periglacial colonization of these two ancestral populations (Figure 6c). Our study demonstrates that even among subpopulations only 500 m apart, the signature of historical glaciation is still observable in contemporary individuals.

4.3 | Gene flow in historical landscape

Our reconstruction of fine-scale spatial-temporal environmental resistance to gene flow between populations addressed three major considerations in landscape genomics: (1) First, we constructed spatially explicit models of populations across six time periods. We reconstructed models of population distribution from moraine records. This approach allowed us to reconstruct historical scenarios as temporally-explicit as the moraine record allowed (five periods in the past 50 kya). These models assume that ancestral populations arrived at their present location in each valley following the receding ice sheets (instead of in situ "nunatak" preservation). If populations had always remained in their current positions, we would find the IBD pattern best explained by contemporary distances between populations. (2) Second, by implementing different criteria for selecting paths along which migration occurs (Euclidean, "avoid glaciers", "least cost", "least resistance"), we contribute to the on-going discussion regarding the best practice to quantify landscape permeability to gene flow (Fant et al., 2014; MacDonald et al., 2020; McRae & Beier, 2007). (3) Third, we applied Bayesian methods to quantify the contribution of environment and geography to genomic divergence (Bradburd et al., 2013), and converted the results into a single measure of distance between populations.

Comparing sets of pair-wise distances generated from a combination of these three considerations allows us to pinpoint historically significant factors affecting *T. shambalaensis* genetic structure. Instead of incorporating results of Mantel/partial Mantel tests in a causal modelling framework to determine the set of distances that best contribute to genetic variation, we specified these distances as

parameters in FASTSIMCOAL2 coalescence to more accurately simulate the "spatial pedigree" between each individual (Bradburd & Ralph, 2019). Compared with coalescent simulations that impose presence/absence of migration, our approach of adjusting the relative number of migrants between populations has the advantage of keeping the number of parameters constant across comparisons. However, a drawback to our approach is the need for sufficient computational resources required to enable coalescent models to converge, if at all, given as many as 50 parameters but only thousands of SNPs. Future studies might compare our approach with models under the integrated distributional, demographic and coalescent framework (iDDC; He et al., 2013). While we mentioned in the introduction that lack of high-resolution environmental niche modeling (ENM) data might affect the application of such a framework on fine-scale landscapes, a work-around under iDDC might involve using the extent of historical ice sheet or elevational data to directly condition key demographic parameters in the model -- thus circumventing the need of ENM. While such an approach would remain computationally demanding and the use of approximate Bayesian computation (ABC) model selection would be challenging, it has the advantage of reducing the number of model parameters.

Along the spatial axis, models using gene flow paths with consideration of environmental resistance and 3D topology outperform models of direct Euclidean paths (Figure 3d). This again highlights the effect of mountainous topology in redefining "distance" among populations. Along the temporal axis, our coalescent models show that contemporary *T. shambalaensis* genetic structure is best explained by gene flow among LGM_L populations (Figure 3c). That is to say, a signature of gene flow among populations in the LGM_L refugium is still preserved today. This is possible because post LGM_L, populations expanded deeper into individual valleys following retreating ice sheets, but during this process, migration between populations was greatly reduced. Our study provides multiple lines of evidence for this "migrate, then expand" scenario:

(1) First, while relative distances between populations fluctuated from past to present, the absolute distance between each population (measured by Euclidean distance, "least cost" distance, "least resistance" distance) increased from past to present (Figure S8). In other words, populations have become more isolated from each other by migrating deeper into the valleys. (2) Second, although migration could be continuously happening at varying rates throughout population history, our direct comparison between pre-resizing migration and post-resizing migration simulations (using the same number of parameters) showed higher support for the former models (Table S5). The timing of migration in the best "preresizing migration" models also corresponds to LGM_L (Table 3a). In terms of resizing dynamics, both FASTSIMCOAL2 and *δaδi* simulations indicate population growth as the best model for individual populations (Table 3). (3) Lastly, contemporary population statistics did not detect deviation from HWE; present-day migration, if any, was not sufficient to be detected statistically.

All these lines of evidence suggest that post-LGM_L *T. shambalaensis* divergence along glacier valleys gradually increased the degree of isolation between populations. If it has not happened already, we suspect that given sufficient time and continued isolation, Dobzhansky-Muller incompatibilities (intrinsic reproductive barriers) will develop among these populations (Orr & Turelli, 2001). Similar mechanisms could explain the contribution of glacier refugia to the generation of insect diversity among the Hengduan Mountains.

ACKNOWLEDGEMENTS

ZW was supported by a graduate fellowship and a Royall Tyler Moore Grant from the Department of Organismic and Evolutionary Biology, Harvard University. NEP was supported by NSF DEB 1541560. We thank Ping Hua, Zulian Zhou, Huailiang Tang from Yanzigou village, Quan Lan, Minxiu Zhang from Moxi County, Ming Liu, Ping Huang, Fulin Liu from Puziba village, for their assistance in the field; this research would not have been possible without their generosity in sharing their knowledge of caterpillar fungus habitats, and we are deeply grateful for their kindness and hospitality. We thank Yongjie Wu, Xue Chen and Xingcheng He from Sichuan University for logistic support. We thank the subject editor Tara Pelletier, reviewer Jared Grummer and two other anonymous reviewers for their constructive comments that greatly improved our original manuscript. ZW thanks John Henry Boyle, Bruno de Medeiros, Benjamin Goulet-Scott and Sofia Prado-Irwin for helpful discussions and for commenting on an early draft of the manuscript, and the members of his thesis committee, Brian Farrell, David Haig and Kamal Bawa for their advice and support. The publication of this research is supported by a grant from the Wetmore Colles Fund, Harvard Museum of Comparative Zoology.

AUTHOR CONTRIBUTIONS

Zhengyang Wang and Naomi E. Pierce conceived of the study. Zhengyang Wang conducted the study, carried out the analysis and wrote the original draft. Both authors prepared the final manuscript.

DATA AVAILABILITY STATEMENT

Raw reads, scripts for running analysis, as well as model parameters have been made accessible on Dryad: https://doi.org/10.5061/dryad.v41ns1rzm.

ORCID

Zhengyang Wang https://orcid.org/0000-0003-3244-1954
Naomi E. Pierce https://orcid.org/0000-0003-3366-1625

REFERENCES

Andrews, K. R., Good, J. M., Miller, M. R., Luikart, G., & Hohenlohe, P. A. (2016). Harnessing the power of RADseq for ecological and evolutionary genomics. *Nature Reviews Genetics*, *17*(2), 81–92. https://doi.org/10.1038/nrg.2015.28

Arnaud, J. F. (2003). Metapopulation genetic structure and migration pathways in the land snail *Helix aspersa*: Influence of landscape heterogeneity. *Landscape Ecology*, *18*, 333–346.

Bagley, R. K., Sousa, V. C., Niemiller, M. L., & Linnen, C. R. (2017). History, geography and host use shape genomewide patterns of genetic variation in the redheaded pine sawfly (*neodiprion lecontei*). *Molecular Ecology*, *26*(4), 1022–1044. https://doi.org/10.1111/mec.13972

Becheler, A., Coron, C., & Dupas, S. (2019). The Quetzal Coalescence template library: A C++ programmers resource for integrating distributional, demographic and coalescent models. *Molecular Ecology Resources*, *19*(3), 788–793. https://doi.org/10.1111/1755-0998.12992

Bemmels, J. B., Title, P. O., Ortego, J., & Knowles, L. L. (2016). Tests of species-specific models reveal the importance of drought in postglacial range shifts of a Mediterranean-climate tree: Insights from integrative distributional, demographic and coalescent modelling and ABC model selection. *Molecular Ecology*, *25*(19), 4889–4906. https://doi.org/10.1111/mec.13804

Bolch, T., Kulkarni, A., Kääb, A., Huggel, C., Paul, F., Cogley, J. G., Frey, H., Kargel, J. S., Fujita, K., Scheel, M., Bajracharya, S., & Stoffel, M. (2012). The state and fate of himalayan glaciers. *Science*, *336*(6079), 310–314. https://doi.org/10.1126/science.1215828

Boyle, J. H., Martins, D., Musili, P. M., & Pierce, N. E. (2019). Population genomics and demographic sampling of the ant-plant *Vachellia drepanolobium* and its symbiotic ants from sites across its range in East Africa. *Frontiers in Ecology and Evolution*, *7*, 206. https://doi.org/10.3389/fevo.2019.00206

Bradburd, G. S., & Ralph, P. L. (2019). Spatial population genetics: It's about time. *Annual Review of Ecology, Evolution, and Systematics*, *50*(1), 427–449. https://doi.org/10.1146/annurev-ecolsys-110316-022659

Bradburd, G. S., Ralph, P. L., & Coop, G. M. (2013). Disentangling the effects of geographic and ecological isolation on genetic differentiation: Isolation by geographic and ecological distance. *Evolution*, *67*(11), 3258–3273. https://doi.org/10.1111/evo.12193

Brown, J. L., & Knowles, L. L. (2012). Spatially explicit models of dynamic histories: Examination of the genetic consequences of Pleistocene glaciation and recent climate change on the American Pika. *Molecular Ecology*, *21*(15), 3757–3775. https://doi.org/10.1111/j.1365-294X.2012.05640.x

Bryant, D., & Moulton, V. (2004). Neighbor-net: An agglomerative method for the construction of phylogenetic networks. *Molecular Biology and Evolution*, *21*(2), 255–265. https://doi.org/10.1093/molbev/msh018

Carstens, B. C., & Richards, C. L. (2007). Integrating coalescent and ecological niche modeling in comparative phylogeography. *Evolution*, *61*(6), 1439–1454. https://doi.org/10.1111/j.1558-5646.2007.00117.x

Catchen, J., Hohenlohe, P. A., Bassham, S., Amores, A., & Cresko, W. A. (2013). Stacks: An analysis tool set for population genomics. *Molecular Ecology*, *22*(11), 3124–3140. https://doi.org/10.1111/mec.12354

Chu, H. F., Wang, L. Y., & Han, H. X. (2004) *Fauna Sinica (Volume 38). Lepidoptera: Hepialidae, Epiplemidae*. Science Press. [in Chinese]

Ciannelli, L., Knutsen, H., Olsen, E. M., Espeland, S. H., Asplin, L., Jelmert, A., Knutsen, J. A., & Stenseth, N. C. (2010). Small-scale genetic structure in a marine population in relation to water circulation and egg characteristics. *Ecology*, *91*(10), 2918–2930. https://doi.org/10.1890/09-1548.1

Clark, P. U., Dyke, A. S., Shakun, J. D., Carlson, A. E., Clark, J., Wohlfarth, B., Mitrovica, J. X., Hostetler, S. W., & McCabe, A. M. (2009). The last glacial maximum. *Science*, *325*, 710–714. https://doi.org/10.1126/science.1172873

Coffman, A. J., Hsieh, P. H., Gravel, S., & Gutenkunst, R. N. (2016). Computationally efficient composite likelihood statistics for demographic inference. *Molecular Biology and Evolution*, *33*(2), 591–593. https://doi.org/10.1093/molbev/msv255

Crookes, S., & Shaw, P. W. (2016). Isolation by distance and non-identical patterns of gene flow within two river populations of the freshwater fish *Rutilus rutilus* (L. 1758). *Conservation Genetics*, *17*(4), 861–874. https://doi.org/10.1007/s10592-016-0828-3

Currat, M., Arenas, M., Quilodràn, C. S., Excoffier, L., & Ray, N. (2019). SPLATCHE3: Simulation of serial genetic data under spatially explicit evolutionary scenarios including long-distance dispersal. *Bioinformatics*, *35*(21), 4480–4483. https://doi.org/10.1093/bioinformatics/btz311

de Medeiros, B. A. S., & Farrell, B. D. (2018). Whole-genome amplification in double-digest RADseq results in adequate libraries but fewer sequenced loci. *PeerJ*, *6*, e5089. https://doi.org/10.7717/peerj.5089

Devitt, T. J., Devitt, S. E. C., Hollingsworth, B. D., McGuire, J. A., & Moritz, C. (2013). Montane refugia predict population genetic structure in the Large-blotched Ensatina salamander. *Molecular Ecology*, *22*(6), 1650–1665. https://doi.org/10.1111/mec.12196

Dijkstra, E. W. (1959). A note on two problems in connexion with graphs. *Numerische Mathematik*, *1*(1), 269–271. https://doi.org/10.1007/BF01386390

Dudaniec, R. Y., Spear, S. F., Richardson, J. S., & Storfer, A. (2012). Current and historical drivers of landscape genetic structure differ in core and peripheral salamander populations. *PLoS One*, *7*(5), e36769. https://doi.org/10.1371/journal.pone.0036769

Escobar García, P., Winkler, M., Flatscher, R., Sonnleitner, M., Krejčíková, J., Suda, J., & Schönswetter, P. (2012). Extensive range persistence in peripheral and interior refugia characterizes Pleistocene range dynamics in a widespread Alpine plant species (*senecio carniolicus*, asteraceae). *Molecular Ecology*, *21*(5), 1255–1270. https://doi.org/10.1111/j.1365-294X.2012.05456.x

Etter, P. D., Bassham, S., Hohenlohe, P. A., Johnson, E. A., & Cresko, W. A. (2011). SNP discovery and genotyping for evolutionary genetics using RAD sequencing. *Methods in Molecular Biology*, *772*, 157–178. https://doi.org/10.1007/978-1-61779-228-1_9

Excoffier, L., Dupanloup, I., Huerta-Sánchez, E., Sousa, V. C., & Foll, M. (2013). Robust demographic inference from genomic and snp data. *PLoS Genetics*, *9*(10), e1003905. https://doi.org/10.1371/journal.pgen.1003905

Fant, J. B., Havens, K., Keller, J. M., Radosavljevic, A., & Yates, E. D. (2014). The influence of contemporary and historic landscape features on the genetic structure of the sand dune endemic, *Cirsium pitcheri* (Asteraceae). *Heredity*, *112*(5), 519–530. https://doi.org/10.1038/hdy.2013.134

Fick, S. E., & Hijmans, R. J. (2017). WorldClim 2: New 1-km spatial resolution climate surfaces for global land areas. *International Journal of Climatology*, *37*(12), 4302–4315. https://doi.org/10.1002/joc.5086

Fordham, D. A., Saltré, F., Haythorne, S., Wigley, T. M. L., Otto-Bliesner, B. L., Chan, K. C., & Brook, B. W. (2017). PaleoView: A tool for generating continuous climate projections spanning the last 21 000 years at regional and global scales. *Ecography*, *40*(11), 1348–1358. https://doi.org/10.1111/ecog.03031

Frichot, E., & François, O. (2015). LEA: An R package for landscape and ecological association studies. *Methods in Ecology and Evolution*, *6*(8), 925–929. https://doi.org/10.1111/2041-210X.12382

Frichot, E., Mathieu, F., Trouillon, T., Bouchard, G., & François, O. (2014). Fast and efficient estimation of individual ancestry coefficients. *Genetics*, *196*(4), 973–983. https://doi.org/10.1534/genetics.113.160572

Geng, Y., Tang, S., Tashi, T., Song, Z., Zhang, G., Zeng, L., Zhao, J., Wang, L. I., Shi, J., Chen, J., & Zhong, Y. (2009). Fine- and landscape-scale spatial genetic structure of cushion rockjasmine, Androsace tapete (Primulaceae), across southern Qinghai-Tibetan Plateau. *Genetica*, *135*(3), 419–427. https://doi.org/10.1007/s10709-008-9290-6

Ghalambor, C. K. (2006). Are mountain passes higher in the tropics? Janzen's hypothesis revisited. *Integrative and Comparative Biology*, *46*(1), 5–17. https://doi.org/10.1093/icb/icj003

Gutenkunst, R. N., Hernandez, R. D., Williamson, S. H., & Bustamante, C. D. (2009). Inferring the joint demographic history of multiple populations from multidimensional SNP frequency data. *PLoS Genetics*, *5*(10), e1000695. https://doi.org/10.1371/journal.pgen.1000695

He, Q., Edwards, D. L., & Knowles, L. L. (2013). Integrative testing of how environments from the past to the present shape genetic structure

across landscapes. *Evolution*, *67*(12), 3386–3402. https://doi.org/10.1111/evo.12159

Helsen, K., Jacquemyn, H., & Honnay, O. (2015). Hidden founder effects: Small-scale spatial genetic structure in recently established populations of the grassland specialist plant *Anthyllis vulneraria*. *Molecular Ecology*, *24*(11), 2715–2728. https://doi.org/10.1111/mec.13207

Hevroy, T. H., Moody, M. L., & Krauss, S. L. (2018). Population genetic analysis reveals barriers and corridors for gene flow within and among riparian populations of a rare plant. *AoB PLANTS*, *10*(1), https://doi.org/10.1093/aobpla/plx065

Hopping, K. A., Chignell, S. M., & Lambin, E. F. (2018). The demise of caterpillar fungus in the Himalayan region due to climate change and overharvesting. *Proceedings of the National Academy of Sciences*, *115*(45), 11489–11494. https://doi.org/10.1073/pnas.1811591115

Huson, D. H., & Bryant, D. (2006). Application of phylogenetic networks in evolutionary studies. *Molecular Biology and Evolution*, *23*(2), 254–267. https://doi.org/10.1093/molbev/msj030

Irving, E., & Hebda, R. (1993). Concerning the origin and distribution of Rhododendrons. *Journal of the American Rhododendron Society*, *47*(3), 139–162.

Janzen, D. H. (1967). Why mountain passes are higher in the tropics. *The American Naturalist*, *101*(919), 233–249. https://doi.org/10.1086/282487

Ji, Y., Ashton, L., Pedley, S. M., Edwards, D. P., Tang, Y., Nakamura, A., Kitching, R., Dolman, P. M., Woodcock, P., Edwards, F. A., Larsen, T. H., Hsu, W. W., Benedick, S., Hamer, K. C., Wilcove, D. S., Bruce, C., Wang, X., Levi, T., Lott, M., … Yu, D. W. (2013). Reliable, verifiable and efficient monitoring of biodiversity via metabarcoding. *Ecology Letters*, *16*(10), 1245–1257. https://doi.org/10.1111/ele.12162

Jombart, T. (2008). Adegenet: A R package for the multivariate analysis of genetic markers. *Bioinformatics*, *24*(11), 1403–1405. https://doi.org/10.1093/bioinformatics/btn129

Jombart, T., Devillard, S., & Balloux, F. (2010). Discriminant analysis of principal components: A new method for the analysis of genetically structured populations. *BMC Genetics*, *11*(1), 94. https://doi.org/10.1186/1471-2156-11-94

Karger, D. N., Conrad, O., Böhner, J., Kawohl, T., Kreft, H., Soria-Auza, R. W., Zimmermann, N. E., Linder, H. P., & Kessler, M. (2017). Climatologies at high resolution for the earth's land surface areas. *Scientific Data*, *4*(1), 170122. https://doi.org/10.1038/sdata.2017.122

Keightley, P. D., Pinharanda, A., Ness, R. W., Simpson, F., Dasmahapatra, K. K., Mallet, J., Davey, J. W., & Jiggins, C. D. (2015). Estimation of the spontaneous mutation rate in *Heliconius melpomene*. *Molecular Biology and Evolution*, *32*(1), 239–243. https://doi.org/10.1093/molbev/msu302

Kidd, D. M., & Ritchie, M. G. (2006). Phylogeographic information systems: Putting the geography into phylogeography. *Journal of Biogeography*, *33*(11), 1851–1865. https://doi.org/10.1111/j.1365-2699.2006.01574.x

Kitamura, K., Nakanishi, A., Lian, C., & Goto, S. (2018). Distinctions in fine-scale spatial genetic structure between growth stages of picea jezoensis carr. *Frontiers in Genetics*, *9*, 490. https://doi.org/10.3389/fgene.2018.00490

Kobayashi, S., Abe, S., Tomita, M., & Matsuki, R. (2018). Fine-scale genetic structure and estimation of gene flow of the Japanese brown frog *Rana japonica* in a Satoyama landscape on the western side of Inba lake, eastern japan. *Current Herpetology*, *37*(1), 11–22. https://doi.org/10.5358/hsj.37.11

Lacey Knowles, L., & Alvarado-Serrano, D. F. (2010). Exploring the population genetic consequences of the colonization process with spatio-temporally explicit models: Insights from coupled ecological, demographic and genetic models in montane grasshoppers. *Molecular Ecology*, *19*(17), 3727–3745. https://doi.org/10.1111/j.1365-294X.2010.04702.x

Lanier, H. C., Massatti, R., He, Q., Olson, L. E., & Knowles, L. L. (2015). Colonization from divergent ancestors: Glaciation signatures on contemporary patterns of genomic variation in Collared Pikas (*Ochotona collaris*). *Molecular Ecology*, *24*(14), 3688–3705. https://doi.org/10.1111/mec.13270

Li, Z., He, Y., Yang, X., Theakstone, W. H., Jia, W., Pu, T., Liu, Q., He, X., Song, B. O., Zhang, N., Wang, S., & Du, J. (2010). Changes of the Hailuogou glacier, Mt. Gongga, China, against the background of climate change during the Holocene. *Quaternary International*, *218*(1–2), 166–175. https://doi.org/10.1016/j.quaint.2008.09.005

Liu, C., Fischer, G., Hita Garcia, F., Yamane, S., Liu, Q., Peng, Y. Q., Economo, E. P., Guénard, B., & Pierce, N. E. (2020). Ants of the Hengduan Mountains: A new altitudinal survey and updated checklist for Yunnan Province highlight an understudied insect biodiversity hotspot. *ZooKeys*, *978*, 1–171. https://doi.org/10.3897/zookeys.978.55767

MacDonald, Z. G., Dupuis, J. R., Davis, C. S., Acorn, J. H., Nielsen, S. E., & Sperling, F. A. H. (2020). Gene flow and climate-associated genetic variation in a vagile habitat specialist. *Molecular Ecology*, *29*(20), 3889–3906. https://doi.org/10.1111/mec.15604

Maczey, N., Dhendup, K., Cannon, P., Hywel-Jones, N., & Rai, T. B. (2010). *Thitarodes namnai* sp. nov. and *T. caligophilus* sp. nov. (Lepidoptera: Hepialidae), hosts of the economically important entomopathogenic fungus *Ophiocordyceps sinensis* in Bhutan. *Zootaxa*, *2412*(1), 42. https://doi.org/10.11646/zootaxa.2412.1.3

Manel, S., Schwartz, M. K., Luikart, G., & Taberlet, P. (2003). Landscape genetics: Combining landscape ecology and population genetics. *Trends in Ecology & Evolution*, *18*(4), 189–197. https://doi.org/10.1016/S0169-5347(03)00008-9

Mantel, N. (1967). The detection of disease clustering and a generalized regression approach. *Cancer Research*, *27*(2), 209–220.

Marchese, C. (2015). Biodiversity hotspots: A shortcut for a more complicated concept. *Global Ecology and Conservation*, *3*, 297–309. https://doi.org/10.1016/j.gecco.2014.12.008

Marske, K. A., Thomaz, A. T., & Knowles, L. L. (2020). Dispersal barriers and opportunities drive multiple levels of phylogeographic concordance in the Southern Alps of New Zealand. *Molecular Ecology*, *29*(23), 4665–4679. https://doi.org/10.1111/mec.15655

Marth, G. T., Czabarka, E., Murvai, J., & Sherry, S. T. (2004). The allele frequency spectrum in genome-wide human variation data reveals signals of differential demographic history in three large world populations. *Genetics*, *166*(1), 351–372. https://doi.org/10.1534/genetics.166.1.351

Massatti, R., & Knowles, L. L. (2016). Contrasting support for alternative models of genomic variation based on microhabitat preference: Species-specific effects of climate change in alpine sedges. *Molecular Ecology*, *25*(16), 3974–3986. https://doi.org/10.1111/mec.13735

Mayr, E. (1942). *Systematics and the Origin of Species*. Columbia University Press.

McRae, B. H. (2006). Isolation by resistance. *Evolution*, *60*(8), 1551–1561. https://doi.org/10.1111/j.0014-3820.2006.tb00500.x

McRae, B. H., & Beier, P. (2007). Circuit theory predicts gene flow in plant and animal populations. *Proceedings of the National Academy of Sciences*, *104*(50), 19885–19890. https://doi.org/10.1073/pnas.0706568104

McRae, B. H., Dickson, B. G., Keitt, T. H., & Shah, V. B. (2008). Using circuit theory to model connectivity in ecology, evolution, and conservation. *Ecology*, *89*(10), 2712–2724. https://doi.org/10.1890/07-1861.1

Meng, L., Chen, G., Li, Z., Yang, Y., Wang, Z., & Wang, L. (2015). Refugial isolation and range expansions drive the genetic structure of Oxyria sinensis (Polygonaceae) in the Himalaya-Hengduan Mountains. *Scientific Reports*, *5*(1), 10396. https://doi.org/10.1038/srep10396

Moreira, L. R., Hernandez-Baños, B. E., & Smith, B. T. (2020). Spatial predictors of genomic and phenotypic variation differ in a lowland Middle American bird (*Icterus gularis*). *Molecular Ecology*, *29*(16), 3084–3101. https://doi.org/10.1111/mec.15536

Myers, E. A., McKelvy, A. D., & Burbrink, F. T. (2020). Biogeographic barriers, Pleistocene refugia, and climatic gradients in the southeastern Nearctic drive diversification in cornsnakes (*Pantherophis guttatus* complex). *Molecular Ecology*, *29*(4), 797–811. https://doi.org/10.1111/mec.15358

Ney, G., Frederick, K., & Schul, J. (2018). A post-pleistocene Calibrated Mutation Rate from Insect Museum Specimens. *PLoS Currents*, *10*. https://doi.org/10.1371/currents.tol.aba557de56be881793261f7e1565cf35

Nosil, P., & Crespi, B. J. (2004). Does gene flow constrain adaptive divergence or vice versa? A test using ecomorphology and sexual isolation in Timema cristinae walking-sticks. *Evolution*, *58*(1), 102–112. https://doi.org/10.1111/j.0014-3820.2004.tb01577.x

Nosil, P., Funk, D. J., & Ortiz-Barrientos, D. (2009). Divergent selection and heterogeneous genomic divergence. *Molecular Ecology*, *18*(3), 375–402. https://doi.org/10.1111/j.1365-294X.2008.03946.x

Orr, H. A., & Turelli, M. (2001). The evolution of postzygotic isolation: Accumulating dobzhansky-muller incompatibilities. *Evolution*, *55*(6), 1085–1094. https://doi.org/10.1111/j.0014-3820.2001.tb00628.x

Orsini, L., Vanoverbeke, J., Swillen, I., Mergeay, J., & De Meester, L. (2013). Drivers of population genetic differentiation in the wild: Isolation by dispersal limitation, isolation by adaptation and isolation by colonization. *Molecular Ecology*, *22*(24), 5983–5999. https://doi.org/10.1111/mec.12561

Ortego, J., Gugger, P. F., & Sork, V. L. (2015). Climatically stable landscapes predict patterns of genetic structure and admixture in the Californian canyon live oak. *Journal of Biogeography*, *42*, 328–338. https://doi.org/10.1111/jbi.12419

Pan, B. T., Zhang, G. L., Wang, J., Cao, B., Geng, H. P., Wang, J., Zhang, C., & Ji, Y. P. (2012). Glacier changes from 1966–2009 in the Gongga Mountains, on the south-eastern margin of the Qinghai-Tibetan Plateau and their climatic forcing. *The Cryosphere*, *6*, 1087–1101. https://doi.org/10.5194/tc-6-1087-2012

Patterson, N., Price, A. L., & Reich, D. (2006). Population structure and eigenanalysis. *PLoS Genetics*, *2*(12), e190. https://doi.org/10.1371/journal.pgen.0020190

Pearson, S. K., Johnston, G. R., Bull, C. M., Fenner, A. L., & Gardner, M. G. (2020). Fine-scale genetic structuring in a group-living lizard, the gidgee skink (*egernia stokesii*): Fine-scale genetics in a group-living lizard. *Austral Ecology*, *45*(4), 435–443. https://doi.org/10.1111/aec.12862

Peres, E. A., DaSilva, M. B., Antunes, M., & Pinto-Da-Rocha, R. (2018). A short-range endemic species from south-eastern Atlantic Rain Forest shows deep signature of historical events: phylogeography of harvestmen *Acutisoma longipes* (Arachnida: Opiliones). *Systematics and Biodiversity*, *16*(2), 171–187. https://doi.org/10.1080/14772000.2017.1361479

Pickrell, J., & Pritchard, J. (2012). Inference of population splits and mixtures from genome-wide allele frequency data. *PLoS Genetics*, *8*(11), e1002967. https://doi.org/10.1371/journal.pgen.1002967

Portik, D. M., Leaché, A. D., Rivera, D., Barej, M. F., Burger, M., Hirschfeld, M., Rödel, M.-O., Blackburn, D. C., & Fujita, M. K. (2017). Evaluating mechanisms of diversification in a Guineo-Congolian tropical forest frog using demographic model selection. *Molecular Ecology*, *26*(19), 5245–5263. https://doi.org/10.1111/mec.14266

Qiu, Y.-X., Fu, C.-X., & Comes, H. P. (2011). Plant molecular phylogeography in China and adjacent regions: Tracing the genetic imprints of Quaternary climate and environmental change in the world's most diverse temperate flora. *Molecular Phylogenetics and Evolution*, *59*(1), 225–244. https://doi.org/10.1016/j.ympev.2011.01.012

Quan, Q.-M., Wang, Q.-X., Zhou, X.-L., Li, S., Yang, X.-L., Zhu, Y.-G., & Cheng, Z. (2014). Comparative phylogenetic relationships and genetic structure of the caterpillar fungus *Ophiocordyceps sinensis* and its host insects inferred from multiple gene sequences. *Journal of Microbiology*, *52*(2), 99–105. https://doi.org/10.1007/s12275-014-3391-y

Rochette, N. C., & Catchen, J. M. (2017). Deriving genotypes from RAD-seq short-read data using Stacks. *Nature Protocols*, *12*(12), 2640–2659. https://doi.org/10.1038/nprot.2017.123

Rottenstreich, S., Hamilton, M. B., & Miller, J. R. (2007). Dynamics of for the island model. *Theoretical Population Biology*, *72*(4), 485–503. https://doi.org/10.1016/j.tpb.2007.08.007

Rousset, F. (1997). Genetic differentiation and estimation of gene flow from *f* -statistics under isolation by distance. *Genetics*, *145*(4), 1219–1228. https://doi.org/10.1093/genetics/145.4.1219

Rutherford, S., Wan, J. S. H., Cohen, J. M., Benson, D., & Rossetto, M. (2021). Looks can be deceiving: Speciation dynamics of co-distributed *Angophora* (Myrtaceae) species in a varying landscape. *Evolution*, *75*(2), 310–329. https://doi.org/10.1111/evo.14140

Schwentner, M., & Giribet, G. (2018). Phylogeography, species delimitation and population structure of a Western Australian short-range endemic mite harvestman (Arachnida: Opiliones: Pettalidae: *Karripurcellia*). *Evolutionary Systematics*, *2*, 81–87. https://doi.org/10.3897/evolsyst.2.25274

Shrestha, B., Tanaka, E., Han, J. G., Oh, J., Han, S. K., Lee, K. H., & Sung, G. H. 2014. A brief chronicle of the genus cordyceps fr., the oldest valid genus in cordycipitaceae (hypocreales, ascomycota). *Mycobiology*, *42*, 93–99. https://doi.org/10.5941/MYCO.2014.42.2.93

Shirk, A. J., Wallin, D. O., Cushman, S. A., Rice, C. G., & Warheit, K. I. (2010). Inferring landscape effects on gene flow: A new model selection framework. *Molecular Ecology*, *19*(17), 3603–3619. https://doi.org/10.1111/j.1365-294X.2010.04745.x

Silva, C. N. S., Murphy, N. P., Bell, J. J., Green, B. S., Duhamel, G., Cockcroft, A. C., Hernández, C. E., & Strugnell, J. M. (2021). Global drivers of recent diversification in a marine species complex. *Molecular Ecology*, *30*(5), 1223–1236. https://doi.org/10.1111/mec.15780

Smith, C. C., Weber, J. N., Mikheyev, A. S., Roces, F., Bollazzi, M., Kellner, K., & Mueller, U. G. (2019). Landscape genomics of an obligate mutualism: Concordant and discordant population structures between the leafcutter ant *Atta texana* and its two main fungal symbiont types. *Molecular Ecology*, *mec.15111*, https://doi.org/10.1111/mec.15111

Stehlik, I., Blattner, F. R., Holderegger, R., & Bachmann, K. (2002). Nunatak survival of the high Alpine plant *Eritrichium nanum* (L.) Gaudin in the central Alps during the ice ages. *Molecular Ecology*, *11*(10), 2027–2036. https://doi.org/10.1046/j.1365-294X.2002.01595.x

Sung, G. H., Hywel-Jones, N. L., Sung, J. M., Luangsa-Ard, J. J., Shrestha, B., & Spatafora, J. W. (2007). Phylogenetic classification of Cordyceps and the clavicipitaceous fungi. *Studies in mycology*, *57*, 5–59. https://doi.org/10.3114/sim.2007.57.01

Tao, Z., Cao, L., Zhang, Y., Ye, Y., & Han, R. (2016). Laboratory rearing of *Thitarodes armoricanus* and *Thitarodes jianchuanensis* (Lepidoptera: Hepialidae), hosts of the Chinese medicinal fungus *Ophiocordyceps sinensis* (Hypocreales: Ophiocordycipitaceae). *Journal of Economic Entomology*, *109*(1), 176–181. https://doi.org/10.1093/jee/tov319

Thomaz, A. T., & Knowles, L. L. (2020). Common barriers, but temporal dissonance: Genomic tests suggest ecological and paleo-landscape sieves structure a coastal riverine fish community. *Molecular Ecology*, *29*(4), 783–796. https://doi.org/10.1111/mec.15357

Van Buskirk, J., & Jansen van Rensburg, A. (2020). Relative importance of isolation-by-environment and other determinants of gene flow in an alpine amphibian. *Evolution*, *74*(5), 962–978. https://doi.org/10.1111/evo.13955

van Etten, J. (2017). R package gdistance: Distances and routes on geographical grids. *Journal of Statistical Software*, *76*(13), https://doi.org/10.18637/jss.v076.i13

van Etten, J., & Hijmans, R. J. (2010). A geospatial modelling approach integrating archaeobotany and genetics to trace the origin and

dispersal of domesticated plants. *PLoS One*, *5*(8), e12060. https://doi.org/10.1371/journal.pone.0012060

van Strien, M. J., Holderegger, R., & Van Heck, H. J. (2015). Isolation-by-distance in landscapes: Considerations for landscape genetics. *Heredity*, *114*(1), 27–37. https://doi.org/10.1038/hdy.2014.62

Vasconcellos, M. M., Colli, G. R., Weber, J. N., Ortiz, E. M., Rodrigues, M. T., & Cannatella, D. C. (2019). Isolation by instability: Historical climate change shapes population structure and genomic divergence of treefrogs in the Neotropical Cerrado savanna. *Molecular Ecology*, *28*(7), 1748–1764. https://doi.org/10.1111/mec.15045

Vieira, M. L. C., Santini, L., Diniz, A. L., de Munhoz, C. F. (2016). Microsatellite markers: What they mean and why they are so useful. *Genetics and Molecular Biology*, *39*(3), 312–328. https://doi.org/10.1590/1678-4685-GMB-2016-0027

Wachter, G. A., Papadopoulou, A., Muster, C., Arthofer, W., Knowles, L. L., Steiner, F. M., & Schlick-Steiner, B. C. (2016). Glacial refugia, recolonization patterns and diversification forces in Alpine-endemic *Megabunus* harvestmen. *Molecular Ecology*, *25*(12), 2904–2919. https://doi.org/10.1111/mec.13634

Wallis, G. P., Waters, J. M., Upton, P., & Craw, D. (2016). Transverse alpine speciation driven by glaciation. *Trends in Ecology & Evolution*, *31*(12), 916–926. https://doi.org/10.1016/j.tree.2016.08.009

Wan, T., Oaks, J. R., Jiang, X.-L., Huang, H., & Knowles, L. L. (2021). Differences in Quaternary co-divergence reveals community-wide diversification in the mountains of southwest China varied among species. *Proceedings of the Royal Society B: Biological Sciences*, *288*(1942), 20202567. https://doi.org/10.1098/rspb.2020.2567

Wang, I. J., Glor, R. E., & Losos, J. B. (2013). Quantifying the roles of ecology and geography in spatial genetic divergence. *Ecology Letters*, *16*(2), 175–182. https://doi.org/10.1111/ele.12025

Wang, I. J., & Summers, K. (2010). Genetic structure is correlated with phenotypic divergence rather than geographic isolation in the highly polymorphic strawberry poison-dart frog. *Molecular Ecology*, *19*(3), 447–458. https://doi.org/10.1111/j.1365-294X.2009.04465.x

Wang, J., Pan, B., Zhang, G., Cui, H., Cao, B., & Geng, H. (2013). Late quaternary glacial chronology on the eastern slope of Gongga Mountain, Eastern Tibetan Plateau, China. *Science China Earth Sciences*, *56*(3), 354–365. https://doi.org/10.1007/s11430-012-4514-0

Wang, X.-L., & Yao, Y.-J. (2011). Host insect species of *Ophiocordyceps sinensis*: A review. *ZooKeys*, *127*, 43–59. https://doi.org/10.3897/zookeys.127.802

Wang, Z., Huang, Y., & Pierce, N. E. (2019). Radio telemetry helps record the dispersal patterns of birdwing butterflies in mountainous habitats: Golden Birdwing (*Troides aeacus*) as an example. *Journal of Insect Conservation*, *23*(4), 729–738. https://doi.org/10.1007/s10841-019-00167-5

Wang, Z., Li, M., Ju, W., Ye, W., Xue, L., Boufford, D. E., Gao, X., Yue, B., Liu, Y., & Pierce, N. E. (2020). The entomophagous caterpillar fungus *Ophiocordyceps sinensis* is consumed by its lepidopteran host as a plant endophyte. *Fungal Ecology*, *47*, 100989. https://doi.org/10.1016/j.funeco.2020.100989

Wang, Z., Zhuang, H., Wang, M., & Pierce, N. E. (2019). Thitarodes shambalaensis sp. nov. (Lepidoptera, hepialidae): A new host of the caterpillar fungus *Ophiocordyceps sinensis* supported by genome-wide SNP data. *ZooKeys*, *885*, 89–113. https://doi.org/10.3897/zookeys.885.34638

Ward, J. H. (1963). Hierarchical grouping to optimize an objective function. *Journal of the American Statistical Association*, *58*(301), 236–244. https://doi.org/10.1080/01621459.1963.10500845

Wegmann, D., Leuenberger, C., Neuenschwander, S., & Excoffier, L. (2010). ABCtoolbox: A versatile toolkit for approximate Bayesian computations. *BMC Bioinformatics*, *11*(1), 116. https://doi.org/10.1186/1471-2105-11-116

Weng, Y., Kavanaugh, D. H., & Schoville, S. D. (2021). Drainage basins serve as multiple glacial refugia for alpine habitats in the Sierra Nevada Mountains. *California. Molecular Ecology*, *30*(3), 826–843. https://doi.org/10.1111/mec.15762

Whitlock, M. C., & McCauley, D. E. (1999). Indirect measures of gene flow and migration: FST≠1/(4Nm+1). *Heredity*, *82*(2), 117–125. https://doi.org/10.1038/sj.hdy.6884960

Winkler, D. (2008). Yartsa Gunbu (*Cordyceps sinensis*) and the fungal commodification of Tibet's rural economy. *Economic Botany*, *62*, 291–305. https://doi.org/10.1007/s12231-008-9038-3

Winkler, D. (2010). *Cordyceps sinensis*: A precious parasitic fungus infecting Tibet. *Field Mycology*, *11*(2), 60–67. https://doi.org/10.1016/j.fldmyc.2010.04.009

Wright, S. (1931). Evolution in mendelian populations. *Genetics*, *16*(3), 290. https://doi.org/10.1093/genetics/16.3.290

Xu, J., Grumbine, R. E., Shrestha, A., Eriksson, M., Yang, X., Wang, Y., & Wilkes, A. (2009). The melting himalayas: Cascading effects of climate change on water, biodiversity, and livelihoods. *Conservation Biology*, *23*(3), 520–530. https://doi.org/10.1111/j.1523-1739.2009.01237.x

Yannic, G., Pellissier, L., Ortego, J., Lecomte, N., Couturier, S., Cuyler, C., Dussault, C., Hundertmark, K. J., Irvine, R. J., Jenkins, D. A., Kolpashikov, L., Mager, K., Musiani, M., Parker, K. L., Røed, K. H., Sipko, T., Þórisson, S. G., Weckworth, B. V., Guisan, A., … Côté, S. D. (2014). Genetic diversity in caribou linked to past and future climate change. *Nature Climate Change*, *4*(2), 132–137. https://doi.org/10.1038/nclimate2074

Zhang, Y., Zhang, S., Li, Y., Ma, S., Wang, C., Xiang, M., Liu, X., An, Z., Xu, J., & Liu, X. (2014). Phylogeography and evolution of a fungal-insect association on the Tibetan Plateau. *Molecular Ecology*, *23*(21), 5337–5355. https://doi.org/10.1111/mec.12940

Ziege, M., Theodorou, P., Jüngling, H., Merker, S., Plath, M., Streit, B., & Lerp, H. (2020). Population genetics of the European rabbit along a rural-to-urban gradient. *Scientific Reports*, *10*(1), 2448. https://doi.org/10.1038/s41598-020-57962-3

Zou, Z.-W., Liu, X., & Zhang, G.-R. (2011). Two new species of Thitarodes (Lepidoptera: Hepialidae) from Tibet in China. *The Pan-Pacific Entomologist*, *87*(2), 106–113. https://doi.org/10.3956/2010-24.1

SUPPORTING INFORMATION

Additional supporting information may be found in the online version of the article at the publisher's website.

How to cite this article: Wang, Z., & Pierce, N. E. (2022). Fine-scale genome-wide signature of Pleistocene glaciation in *Thitarodes* moths (Lepidoptera: Hepialidae), host of *Ophiocordyceps* fungus in the Hengduan Mountains. *Molecular Ecology*, *00*, 1–20. https://doi.org/10.1111/mec.16457